LBL-38540
UC-405

Lawrence Berkeley Laboratory
UNIVERSITY OF CALIFORNIA

Physics Division

Mathematics Department

To be submitted for publication

On the Motion of Slender Vortex Filaments

H. Zhou

April 1996

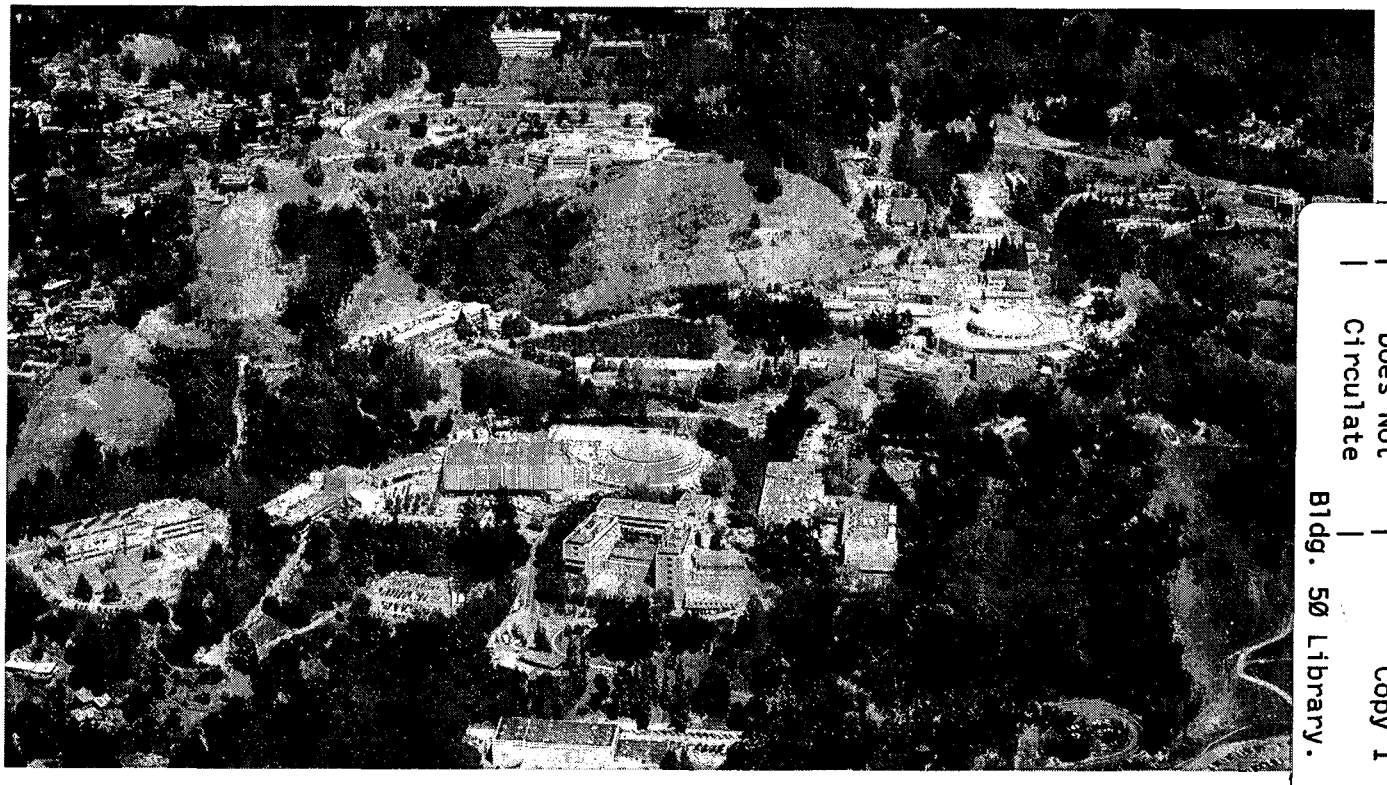

Prepared for the U.S. Department of Energy under Contract Number DE-AC03-76SF00098

DISCLAIMER

LBL-38540

On the motion of slender vortex filaments *

Hong Zhou

Department of Mathematics
and
Lawrence Berkeley National Laboratory
University of California
Berkeley, CA 94720, USA

April 1996

* This work was supported in part by the Applied Mathematical Sciences subprogram of the Office of Energy Research, U.S. Department of Energy, under Contract Number DE-AC03-76SF00098.

Abstract

Several numerical methods for slender vortex motion (the local induction equation, the Klein-Majda equation, and the Klein-Knio equation) are compared on the specific example of sideband instability of Kelvin waves on a vortex. Numerical experiments on this model problem indicate that all these methods yield qualitatively similar behavior, and this behavior is different from the behavior of a non-slender vortex with variable cross-section. It is found that the boundaries between stable, recurrent, and chaotic regimes in the parameter space of the model problem depend on the method used. The boundaries of these domains in the parameter space for the Klein-Majda equation and for the Klein-Knio equation are closely related to the core size. When the core size is large enough, the Klein-Majda equation always exhibits stable solutions for our model problem. Various conclusions are drawn; in particular, the behavior of turbulent vortices cannot be captured by these approximations, and probably cannot be captured by any slender vortex model with constant vortex cross-section. Speculations about the differences between classical and superfluid hydrodynamics are also offered.

1 Introduction

Fluid vorticity is often concentrated in small regions. The special case where vorticity is concentrated on a single slender filament is important in many problems (e.g. turbulence, superfluidity). The study of the motion of slender vortices has received a lot of attention. The local induction equation [1], the Klein-Majda equation [2], and the Klein-Knio equation [3] are three different approximations for the motion of slender vortices. The comparison of these methods and the study of differences between the results and what we expect in turbulence theory are the main goals of this paper.

The paper is organized as follows. After a brief review of vortex dynamics, we present approximate equations of motion for slender vortices, namely, the self-induction equation, the Klein-Majda equation and the Klein-Knio equation. The third section describes a model problem which comes from the theory of vortex wave motion in superfluid helium. The methods are applied to the model problem, and the results are displayed. We then draw various conclusions from these results.

We consider unbounded, inviscid, incompressible flows. In the absence of external force, the motion of such fluid with unit density is described by the Euler equations:

$$\frac{D\mathbf{u}}{Dt} = -\nabla \mathrm{p}, \tag{1}$$

$$\nabla \cdot \mathbf{u} = 0, \tag{2}$$

where $\mathbf{u}(\mathbf{x},t)$ is the velocity, $\mathbf{x} = (x_1, x_2, x_3)$ is the position, p is the pressure, $\nabla = (\partial/\partial x_1, \partial/\partial x_2, \partial/\partial x_3)$ is the differentiation vector, t is the time, and $D/Dt \equiv \partial_t + \mathbf{u} \cdot \nabla$ is the material derivative.

The curl of the velocity field,

$$\omega = \nabla \times \mathbf{u} \tag{3}$$

is the vorticity. The velocity $\mathbf{u}(\mathbf{x})$ can be determined from the vorticity $\omega(\mathbf{x})$ through the Biot-Savart law :

$$\mathbf{u}(\mathbf{x}) = -\frac{1}{4\pi}\int \frac{(\mathbf{x}-\mathbf{x}')\times\omega(\mathbf{x}')}{|\,\mathbf{x}-\mathbf{x}'\,|^3}dx'. \tag{4}$$

If the vorticity is concentrated on a single thin filament C of circulation Γ, equation (4) becomes

$$\mathbf{u}(\mathbf{x}) = -\frac{\Gamma}{4\pi}\int_C \frac{(\mathbf{x}-\mathbf{x}')\times d\mathbf{l}(\mathbf{x}')}{|\,\mathbf{x}-\mathbf{x}'\,|^3}. \tag{5}$$

If self-induced motion of the line filament is calculated by evaluating the velocity from (5) on the filament itself, the result will be logarithmically infinite if the filament is curved and zero if it is straight. Thus, self-induced motion occurs only for curved filaments. But to obtain the correct value for the velocity, further considerations of the finite size of the vortex core as well as the vorticity distribution are required.

In this paper we focus our attention on very thin vortex filaments. We shall use the term *thin* or *slender* to describe any vortex filament with a typical radius of the core that is small compared to a characteristic radius of curvature. Thin vortices are very important in many respects. It has been suggested by Chorin and Akao [4] that thin vortices play an important role in the structure of turbulent flows.

Vortex motion in three-dimensional space differs from vortex motion in two dimensions in several ways; the most significant result from vortex stretching [5]. Vortex stretching causes vortex folding and the temperature is decreased [6],[7]. As time $t \to \infty$, a statistically steady state can be expected for a vortex filament system [8],[9].

2 Equations of Motion for Thin Vortices

To simulate the motion of a slender vortex filament, using a vortex method would be dramatically expensive. Therefore, approximate equations are developed to replace the Biot-Savart law. Three modeling approaches are used in this section to analyze the motion of slender vortex filaments. The first is the local induction approximation (LIA), which leads to a cubic nonlinear Schrödinger equation. The second is due to Klein and Majda, who derived a more accurate asymptotic equation for the motion of thin vortex filaments. The third approach, due to Klein and Knio, is a three-dimensional simulation based on a vortex element method. It should be pointed out that all three equations assume that the core size is small compared with the radius of curvature. According to the stability analysis given by Widnall et al [10], instability occurs when the wavelength is comparable with the core size of the vortex filament. Therefore, it is plausible to conjecture that hairpins might not develop when the core size is very small, even though Klein and Majda [13] claimed that hairpins appear in their model.

To start with, consider a vortex filament described by $\mathbf{r}(s)$, where s is an arc length parameter measured along the filament and $\mathbf{r}(s)$ is the position vector. Let $\mathbf{t}$, $\mathbf{n}$, $\mathbf{b}$ denote the unit tangent, normal, and binormal vectors, respectively.

One way to avoid singularity in equation (5) is to simply ignore the nonlocal contribution of the filament and replace the Biot-Savart law (5) by a different fluid velocity that depends only on a local curvature of the vortex filament. This leads to the local induction

approximation, which reads [1]

$$\frac{\partial \mathbf{r}}{\partial t} = \mathbf{t} \times \frac{\partial \mathbf{t}}{\partial s} = \kappa \mathbf{b}, \tag{6}$$

where κ is the curvature. Equation (6) has a very different character from the Euler equations, and in particular it preserves vortex length [11].

Differentiation of both sides of (6) with respect to s gives the local induction equation in terms of the tangent vector:

$$\frac{\partial \mathbf{t}}{\partial t} = \mathbf{t} \times \frac{\partial^2 \mathbf{t}}{\partial s^2}. \tag{7}$$

Hasimoto [12] has shown elegantly that equation (6) can be reduced to a cubic nonlinear Schrödinger equation (NLSE)

$$\frac{1}{i}\frac{\partial \phi}{\partial t} = \frac{\partial^2 \phi}{\partial s^2} + \frac{1}{2}\phi \mid \phi \mid^2 \tag{8}$$

where t is the time, s is the length measured along the filament, ϕ is the complex function defined in terms of the filament curvature κ and torsion τ:

$$\phi = \kappa \ \exp(i \int_0^s \tau ds). \tag{9}$$

We call (9) the *Hasimoto transformation* and ϕ the *filament function* which contains all the geometrical information for the filament.

While the local induction approximation does not allow for any vortex stretching, numerical simulations indicate that vortex stretching occurs for moderately thin vortex filaments in incompressible fluids. To retain vortex stretching, Klein and Majda [2] developed an asymptotic theory for slender vortex filaments.

The slender vortices in Klein-Majda regime are, to leading order, straight vortex filaments that are subject to small amplitude displacements. The displacement of the vortex filament

centerlines away from the straight reference lines may be, but is not necessarily, large in comparison with a typical core size of the filament but it must be small compared to a typical perturbation wave length. In turn, the perturbation wavelengths are small compared to a characteristic radius of curvature of the filament. Thus with lengths measured on the curvature scale, the slender vortices in Klein-Majda regime are characterized by *small amplitude - short wavelength* distortions of a slender columnar vortex.

Assume the centerline of a slender vortex filament is described by

$$\mathbf{x}(s,t;\varepsilon) = \varepsilon\sigma\mathbf{t}_0 + \varepsilon^2\mathbf{x}^{(2)}(\sigma,\tau) + o(\varepsilon^2) \tag{10}$$

where $\mathbf{x}$ is the position vector, s is the arc length along the curve, t is the time, $\sigma = s/\varepsilon$ and $\tau = t/\varepsilon^2$ are the scaled space and time coordinates, $\mathbf{t}_0$ is a constant unit vector, ε is a perturbation scaling parameter and $\varepsilon << 1$. The vortex core size δ and ε are linked through the distinguished limit

$$\varepsilon^2 = \frac{1}{\ln\frac{2\varepsilon}{\delta} + C} \tag{11}$$

where C is some constant.

When the far-field flow surrounding the filament is at rest, the filament motion obeys the perturbed binormal law

$$\frac{\partial\mathbf{x}(s,t)}{\partial t} = \kappa\mathbf{b}(s,t) + \varepsilon^2\mathbf{v}(s,t) \tag{12}$$

where $\varepsilon^2\mathbf{v}(s,t)$ is a small perturbation velocity. Using the curve representation (10) and by the method of asymptotic expansions, one finds

$$\mathbf{v} = I[\mathbf{x}^{(2)}] \times \mathbf{t}_0. \tag{13}$$

Here $I[\cdot]$ is the linear nonlocal operator

$$I[w](\sigma) = \int_{-\infty}^{\infty} \frac{1}{|h^3|} \left[w(\sigma + h) - w(\sigma) - hw'(\sigma + h) + \frac{h^2}{2} H(1 - |h|) w''(\sigma) \right] dh \qquad (14)$$

with the notation $' = \partial/\partial\sigma$ and H is the Heaviside function. Therefore, the nonlocal contribution of the filament is replaced by I, whose effect can be understood by considering its Fourier symbol:

$$\begin{aligned} \hat{I}(\xi) &= \int_{\mathbf{R}} e^{-i\sigma\xi} I(\sigma) d\sigma \\ &= |\xi|^2 (-\ln|\xi| + C_0) \end{aligned} \qquad (15)$$

where $C_0 = 1/2 - \gamma$, and γ is Euler's constant.

Klein and Majda showed that Hasimoto's transformation (9) turns the evolution equation (12) with $\mathbf{v}$ from (13) into the perturbed nonlinear-nonlocal Schrödinger equation

$$\frac{1}{i} \frac{\partial \phi}{\partial \tau} = \frac{\partial^2 \phi}{\partial \tilde{\sigma}^2} + \varepsilon^2 (\frac{1}{2} \phi |\phi|^2 - I[\phi]) \qquad (16)$$

with $\tau = t/\varepsilon^2$ and $\tilde{\sigma} = s/\varepsilon$. We call (16) the *Klein-Majda equation.* In this equation, the nonlocal term $I[\phi]$ directly competes with the cubic nonlinearity. Thus, the nonlocal contributions become as important as the nonlinear local induction effects. Furthermore, it is shown that the nonlocal term $-\varepsilon^2 I[\phi]$ is responsible for filament local self-stretching. It is also shown in Klein and Majda [2] that the nonlocal operator generates a highly singular perturbation of the NLSE (8). According to the numerical calculations presented in Klein and Majda [13], the filament function ϕ develops higher and much narrower peaks as time evolves when compared with the corresponding solutions of NLSE; and these curvature peaks may correspond to the birth of small scale "hairpins" or kinks along the actual vortex filament.

Recently Klein and Knio [3] derived an asymptotically correct representation of the non-local induction effects, which is based on a thin-tube model. This method represents the influence of the vortex core structure on the vortex filament motion, including a nontrivial axial flow.

The standard thin-tube model [14] is a simplified version of general vortex element method [15] for three-dimensional incompressible flows. The model represents a slender vortex as a single chain of overlapping vortex elements. Each element is a circular cylinder characterized by a circulation Γ_i equal to the flux of vorticity across its cross section and by two Lagrangian variables which describe the endpoints of the associated line segment. The Lagrangian variables are moving with the fluid and can be denoted by χ_i, $i = 1, 2, ..., N$. The vortex elements are ordered so that the indices increase in the direction of the vorticity. Therefore, the vorticity can be discretized as

$$\omega(\mathbf{x}, t) = \sum_{i=1}^{N} \Gamma_i \delta\chi_i(t) f_\delta(\mathbf{x} - \chi_i^c(t)). \tag{17}$$

In this expression, f_δ is a smooth approximation to the Dirac delta function with a cutoff radius δ and obeys the relationship:

$$f_\delta(\mathbf{x}) = \frac{1}{\delta^3} f(\frac{|\mathbf{x}|}{\delta}), \tag{18}$$

and

$$\delta\chi_i(t) = \chi_{i+1}(t) - \chi_i(t), \tag{19}$$

$$\chi_i^c(t) = \frac{\chi_{i+1}(t) + \chi_i(t)}{2}, \tag{20}$$

denote respectively the length and center of the i-th vortex element. The smoothing function $f(\mathbf{x})$ is chosen so as to enhance accuracy [15]. The velocity at a point $\mathbf{x}$ can be obtained by

inserting (17) into (5) and performing the integration. The result is the following desingularized version of the Biot-Savart law:

$$\mathbf{u}^{\mathrm{ttm}}(\mathbf{x},t) = -\frac{1}{4\pi}\sum_{i=1}^{N}\Gamma_i \frac{(\mathbf{x}-\chi_i^c(t))\times\delta\chi_i^c(t)}{\mid \mathbf{x}-\chi_i^c(t)\mid^3} K_\delta(\mathbf{x}-\chi_i^c(t)) \tag{21}$$

where

$$K_\delta(\mathbf{x}) \equiv K(\frac{|\mathbf{x}|}{\delta}) \tag{22}$$

and $K(r)$ is the velocity smoothing kernel corresponding to the vorticity smoothing kernel:

$$K(r) = 4\pi\int_0^r \bar{r}^2 f(\bar{r})d\bar{r}. \tag{23}$$

The calculated velocity $\mathbf{u}^{\mathrm{ttm}}(\chi_i)$ is used to advance χ_i.

In the above standard thin-tube approach the cutoff radius is implicitly assumed to be the physical characteristic vortex core radius. Klein and Knio found that this assumption is in general incorrect because of the differences between the physical and numerical core structures [3]. To modify the standard thin-tube model, Klein and Knio derive an asymptotic expression for the induced velocity.

In the derivation of the Klein-Knio equation, the principal assumption is that the slender vortex filament has the following core vorticity distribution in curvilinear coordinate system:

$$\begin{aligned}\boldsymbol{\omega}(\mathbf{x},t;\delta) &= \frac{1}{\delta^2}\left(\eta^{(0)}(\frac{r}{\delta},s,t)\mathbf{e}_\theta + \zeta^{(0)}(\frac{r}{\delta},s,t)\mathbf{t}\right)\\ &+ \frac{1}{\delta}\left(\xi^{(1)}(\frac{r}{\delta},\theta,s,t)\mathbf{e}_r + \eta^{(1)}(\frac{r}{\delta},\theta,s,t)\mathbf{e}_\theta + \zeta^{(1)}(\frac{r}{\delta},\theta,s,t)\mathbf{t}\right)\\ &+ O(1)\end{aligned} \tag{24}$$

where δ, the ratio of the core size and the radius of curvature, is a dimensionless parameter, $\xi^{(i)}$, $\eta^{(i)}$, $\zeta^{(i)}$ are asymptotic expansion functions for the radial, circumferential and axial

vorticity components in the vortex core. Notice that the leading order terms $\eta^{(0)}$, $\zeta^{(0)}$ are assumed to be independent of θ so that the leading order core structure is axisymmetric.

Let $\mathbf{u}^{\mathrm{ttm}}$ denote the velocity obtained from the standard thin-tube model, C, C^{ttm} the physical and numerical core structure coefficients, κ the curvature, $\mathbf{b}$ the binormal vector. The three different modifications of the thin-tube model derived by Klein and Knio can be generalized into the following form

$$\mathbf{u} = \mathbf{u}^{\mathrm{ttm}} + \frac{\Gamma}{4\pi}(C^{\mathrm{ttm}} - C + \ln\frac{\delta^{\mathrm{ttm}}}{\delta})\kappa\mathbf{b}, \tag{25}$$

which we name the *Klein-Knio equation.*

If δ^{ttm} is chosen to be δ, then

$$\mathbf{u} = \mathbf{u}^{\mathrm{ttm}} + \frac{\Gamma}{4\pi}(C^{\mathrm{ttm}} - C)\kappa\mathbf{b}. \tag{26}$$

Therefore, when we use the standard thin-tube model with $\delta^{\mathrm{ttm}} = \delta$, we have to add an explicit correction velocity to the numerical velocity $\mathbf{u}^{\mathrm{ttm}}$.

If δ^{ttm} is chosen so that $C^{\mathrm{ttm}} - C + \ln(\delta^{\mathrm{ttm}}/\delta) = 0$, then $\mathbf{u} = \mathbf{u}^{\mathrm{ttm}}$. In other words, if we use a rescaled numerical core radius $\delta^{\mathrm{ttm}} = \delta\exp(C - C^{\mathrm{ttm}})$, the standard thin-tube model can be applied directly without correction. This method is very attractive when δ is small and $\exp(C - C^{\mathrm{ttm}})$ is large. However, (25) is more general and is preferred when δ is extremely small.

3 Numerical Solutions of the Approximate Equations

The method we use to solve the local induction approximation is due to Buttke [11] which is based on equation (7).

Let $\mathbf{t}_j^n$ denote the approximation to $\mathbf{t}(j\Delta s, n\Delta t)$. Buttke developed a Crank-Nicholson type scheme:

$$\mathbf{t}_j^{n+1} - \mathbf{t}_j^n = \frac{\Delta t}{4(\Delta s)^2}\ (\mathbf{t}_j^{n+1} + \mathbf{t}_j^n) \times (\mathbf{t}_{j+1}^{n+1} + \mathbf{t}_{j-1}^{n+1} + \mathbf{t}_{j+1}^n + \mathbf{t}_{j-1}^n) \tag{27}$$

where Δs is the spatial increment, Δt is the temporal increment and the term $\mathbf{t}_j^{n+1} + \mathbf{t}_j^n$ has been cancelled by the first term in the cross product.

The equation (27) can be solved by two iterative methods. Both methods produce a sequence of unit vectors $\mathbf{x}_j^k$ which converges to $\mathbf{t}_j^n$, provided Δt is appropriately restricted.

In the first iterative method, given unit vector $\mathbf{t}_j^n$, we define $\mathbf{y}_j^{k+1}$ by the equation

$$\mathbf{y}_j^{k+1} - \mathbf{t}_j^n = \frac{\Delta t}{4(\Delta s)^2}(\mathbf{x}_j^k + \mathbf{t}_j^n) \times (\mathbf{x}_{j+1}^k + \mathbf{x}_{j-1}^k + \mathbf{t}_{j+1}^n + \mathbf{t}_{j-1}^n) \tag{28}$$

and then define

$$\mathbf{x}_j^{k+1} \equiv \frac{\mathbf{y}_j^{k+1}}{|\ \mathbf{y}_j^{k+1}\ |}. \tag{29}$$

It can be shown [16] that $\mathbf{x}_j^n \longrightarrow \mathbf{t}_j^{n+1}$ if $\Delta t < (\Delta s)^2/4$.

In the second iterative method, we define the sequence of unit vectors $\mathbf{x}_j^k$ by

$$\mathbf{x}_j^{k+1} - \mathbf{t}_j^n = \frac{\Delta t}{4(\Delta s)^2}(\mathbf{x}_j^{k+1} + \mathbf{t}_j^n) \times (\mathbf{x}_{j+1}^k + \mathbf{x}_{j-1}^k + \mathbf{t}_{j+1}^n + \mathbf{t}_{j-1}^n). \tag{30}$$

The sequence $\mathbf{x}_j^k$ obtained in this manner [16] converges to $\mathbf{t}_j^{n+1}$ if $\Delta t < (\Delta s)^2$.

A fractional step method developed by Klein and Majda [13] is used to solve the Klein-Majda equation. The method is designed for general periodic initial data. It consists of two steps. In one fractional step, solve the linear problem

$$\frac{1}{i}\frac{\partial \phi}{\partial \tau} = \frac{\partial^2 \phi}{\partial \tilde{\sigma}^2} - \varepsilon^2 I[\phi] \tag{31}$$

exactly. Through discrete fast Fourier transform (DFFT) of the data for ϕ on an equi-distance grid, one obtains the Fourier modes $\hat{\phi}_l$, $l = -N/2,...,N/2-1$. Then applying the exact solution formula

$$\hat{\phi}_l(\tau + \triangle\tau) = \hat{\phi}_l(\tau)\exp(-i[l^2 + \varepsilon^2 \hat{I}(l)]\triangle\tau) \tag{32}$$

and using the inverse Fourier transform (IFFT) gives the solution of (31).

In the second fractional step, solve the nonlinear ODE

$$\frac{1}{i}\frac{\partial \phi}{\partial \tau} = \varepsilon^2 \frac{1}{2}\phi \mid \phi \mid^2 \tag{33}$$

exactly at each discrete spatial location by

$$\phi_l(\tau + \triangle\tau) = \phi_l(\tau)\exp(i\varepsilon^2 \frac{1}{2} \mid \phi_j(\tau) \mid^2 \triangle\tau). \tag{34}$$

The two steps are alternated in time through Strang-type splitting. The method is second order accurate and unconditionally stable. An adaptive time step $\triangle\tau$ is chosen by

$$\triangle\tau = s\frac{2\pi}{w^*}\frac{1}{N}, \tag{35}$$

where s is a safety factor (say s = 0.5), N is the number of grid points and w^* is the weighted average frequency

$$w^* = \max(-\int \hat{w}(\xi) \mid \hat{\phi} \mid^2 (\xi)d\xi/\|\phi\|^2_{L^2}, \int w(\mid \phi \mid) \mid \hat{\phi} \mid^2 d\sigma/\|\phi\|^2_{L^2}) \tag{36}$$

and $\hat{w}$, w are the frequencies in the fractional step solution formulas in (32) and (34).

Once the filament function $\phi(s,t)$ is known, one can determine the filament position using the Serret-Frenet equations.

We use a hybrid of a fractional step method and a high order Runge-Kutta method to solve the Klein-Knio equation. In one fractional step, solve

$$\frac{d\mathbf{x}}{dt} = \mathbf{u}^{\text{ttm}} \tag{37}$$

by an embedded Runge-Kutta method [17] for one step with controlled step size $\triangle t$. In the second fractional step, solve

$$\frac{d\mathbf{x}}{dt} = \frac{\Gamma}{4\pi}(\kappa\mathbf{b})[C - C^{\text{ttm}} + \ln\frac{\delta^{\text{ttm}}}{\delta}] \tag{38}$$

by the same embedded Runge-Kutta method for several time steps until the sum of the time steps is equal to $\triangle t$. As before, the two steps are alternated in time through Strang-type splitting.

4 A Model Problem

To examine the equations for slender vortex motion, we want to apply them to a well-understood model problem. Our problem comes from the theory of superfluid vortices [21], chosen because of the wealth of analytical results available.

Superfluid helium at absolute zero temperature is inviscid and irrotational. The circulation around a vortex core is quantized and the core radius of superfluid vortices is very small ($O(1\text{Å})$). Vortex waves are a very important phenomenon in the understanding of

quantized vortex lines. Wave excitations of isolated vortex lines in superfluid are considered to be helical disturbances which rotate about the axis of symmetry with a known frequency. When these two helical waves are excited on a vortex line between fixed boundaries, two waves of opposite polarization combine to form a plane standing wave called a Kelvin wave.

Benjamin and Feir [18] showed that finite-amplitude waves on deep water are unstable to perturbations in the sideband waves (i.e. modes whose number of half waves are $n \pm k$, with $k = 1, 2, ...$ and n the number of half waves for the main harmonic). The Benjamin-Feir instabilities are widespread and play an important role in nonlinear wave phenomena. In particular, Yuen and Ferguson [19] have shown that the Benjamin-Feir instabilities appear in the wave solutions to the NLSE. Since helical waves in our problem are wave solutions to the NLSE, it is not surprising that the Benjamin-Feir instabilities occur for Kelvin waves. Following the stability analysis of Andersen, Datta, and Gunshor [20], Samuel and Donnelly [21] found that the stability condition for helical waves which obeys the NLSE is

$$a_0/\lambda < 1/(2\pi n), \tag{39}$$

where a_0 is the initial amplitude of the main helical wave, λ is the wavelength, and n is the number of half waves on the vortex. The stability condition (39) can also be obtained by a linear stability analysis following Klein and Majda [13].

The amplitudes of the unstable sidebands grow exponentially when a_0/λ violates the stability condition (39). Once the amplitudes of the sidebands grow to be comparable in magnitude to the amplitude of the main wave, this instability analysis is invalid and a new behavior occurs. More specifically, when the initial amplitude a_0/λ is smaller than the threshold value given by (39, the amplitudes of the main harmonic and the sidebands don't

grow. We obtain *stable* phenomena. If the initial a_0/λ is increased, the amplitudes of the sidebands start to grow due to Benjamin-Feir instabilities. However, after some time the amplitude of the main harmonic begins to grow and the amplitudes of the sidebands decline. The main harmonic and the sidebands grow or decay alternatively and the process repeats itself although not with perfect periodicity. This kind of phenomenon is normally referred as the *Fermi-Pasta-Ulam recurrence* [22], as opposed to Poincaré recurrence, which requires the return of both amplitude and phase to their initial states. A further increase in the initial value a_0/λ leads a behavior which is neither stable nor recurrent, which can be called *chaotic*. Those behaviors will be illustrated numerically in the following section.

5 Numerical Simulations

We choose the same problem as in Samuels and Donnelly [21]. The initial conditions are chosen as a vortex line extended between two parallel planes 10^{-5} m apart and the vortex line being a superposition of a planar wave and two neighboring sidebands of small amplitude as a perturbation. The boundary conditions are that the vortex line must meet the boundaries perpendicularly and can slip along the boundaries. These conditions can be met by the method of images; one can extend the vortex filament between the boundaries and obtain periodic boundary conditions. In our numerical simulations, as we advance the vortex filament in time, we take the wave form of the filament and obtain the amplitudes of the main mode and its sidebands.

In Figure 1 we present the results given by the self-induction equation. The x-axis is the

time, whereas the y-axis is the ratio of the amplitude and wavelength λ. Plotted are the amplitude of the main harmonic ($n = 11$) and the lower harmonics ($n = 10$, 9, 8 in order of decreasing amplitude) as a function of time. A plot of the upper harmonics ($n = 12$, 13, 14) looks very similar. When the ratio of the amplitude of the main harmonic a_0 and its wavelength λ is 0.02 initially, the amplitudes of the sideband waves don't grow (Figure 1 (a)) and we obtain stable phenomena. If the initial a_0/λ is increased to 0.03 (Figure 1 (b)) or 0.04 (Figure 1 (c)), a recurrent behavior is presented. When a_0/λ is further increased to 0.08 (Figure 1 (d)), a chaotic behavior occurs. These results confirm the stability condition (39). During the evolution of the filament, the total arclength is conserved. In the calculations which lead to Figure 1, we used $N = 257$ nodes to represent the vortex filament between the walls; equation (7) was integrated using a midpoint rule.

The numerical results given by the Klein-Majda model for $a_0/\lambda = 0.02$, 0.03, 0.04, and 0.06 at time $t = 0$ are shown in Figure 2 (a), (b), (c), and (d). Stable, recurrent, and chaotic behaviors are also observed here. Figure 2 was obtained with $N = 257$, and $\varepsilon = 0.309$, which is related to the core size through the distinguished limit (11).

Figure 3 (a), (b), (c), and (d) display the results by the Klein-Knio model corresponding to different initial values of $a_0/\lambda = 0.03$, 0.04, 0.06, and 0.08. Again, stable, recurrent, and chaotic behaviors are exhibited. The evolution of the vortex filament by the Klein-Knio equation keeps the total arclength almost a constant. The results in Figure 3 were obtained with $N = 513$ and $\delta^{\mathrm{ttm}} = 0.01$.

The above numerical experiments indicate that the self-induction equation, the Klein-Majda model, and the Klein-Knio model yield qualitatively similar results for our model

problem. However, they do have some quantitative differences. The boundaries between stable, recurrent, and chaotic regimes in the parameter space (i.e. initial values of a_0/λ) of the methods are different. A comparison of Figure 3 (a) and Figure 1 (b) shows that the Klein-Knio equation has larger stability region than that of the self-induction equation, since for the same initial value $a_0/\lambda = 0.03$, the self-induction equation gives unstable (recurrent) behavior, whereas the Klein-Knio model gives stable behavior. Further numerical experiments also reveal that the stability region of the Klein-Knio model is related to the core size: A larger core size generates a larger stability region.

To compare the self-induction equation and the Klein-Majda model, we plot the stability diagram for both the Klein-Majda model and the NLSE in Figure 4 for $\varepsilon = 0.5$ (Figure 4 (a)), 0.4778 (Figure 4 (b)), 0.309 (Figure 4 (c)), and 0.1 (Figure 4 (d)). The solid lines are for the Klein-Majda model and the dashed lines are for the NLSE. The horizontal axis is a_0/λ, where a_0 is the initial amplitude of the main cosine wave, λ is its wavelength. The vertical axis is the growth rate G. Instability occurs for negative G. As shown in Figure 4, the stability behavior of the Klein-Majda model depends on the parameter ε. More precisely, if $\varepsilon > 0.4778$, the Klein-Majda model always gives stable behavior. When ε is further decreased, the Klein-Majda model has smaller stable region than that of the NLSE. As ε decreases, the stability region of the Klein-Majda model eventually converges to that of the NLSE. For our model problem, the parameter ε is approximately 0.309, hence the self-induction equation has a larger stability region than that of the Klein-Majda model.

For comparison purposes, we use standard vortex method [23], which uses several vortex filaments with overlapping cores, to examine the behavior for the vortex filament. We used 7

vortex filaments to represent the cross-section of the vortex filament, each of which initially having the same shape of Kelvin waves and having 200 segments. The calculation is terminated if there is a filament with more than 1000 segments. A fourth-order Runge-Kutta method was used to advance the filaments with $\triangle t$ controlled by $\triangle t \cdot \max|\mathbf{u}_i^n| \leq Ch$, where $\mathbf{u}_i^n$ is the velocity at the i-th node, C is some constant, h is the spatial step size. Figure 5 depicts perspective views of the vortex at time $t = 0.4216$, 0.8198, 1.5787 and 1.9189. Here the initial value a_0/λ is taken as 0.04. Violent stretching happens very quickly. Figure 6 is another view of Figure 5. The view is generated by projecting the vortex lines on the yz-plane. It is clear that the cross-section is no longer unchanged. We plot the evolution of the modes $n = 8$, 9, 10 and 11 in Figure 7 with different initial data $a_0/\lambda = 0.02$, 0.04, 0.06, 0.08. The solid curve denotes the amplitude of mode $n = 11$, dashed curve $n = 10$, dashdotted curve $n = 9$, and dotted curve $n = 8$. These results show that classical vortex does not present the same dynamical phenomena as the superfluid vortex. Instead, classical vortex seems to present some kind of chaotic behaviors. Our numerical experiments indicate that thick vortices with variable cross-section behave differently from thin vortices with constant cross-section.

In all of our numerical calculations, we have carefully checked that our choices of numerical parameters provide an adequate resolution and that further refinement does not change the conclusions. The oscillations presented in the graphs may originate from the numerical noises.

6 Conclusions

We have used three different methods, namely the self-induction equation, the Klein-Majda equation, and the Klein-Knio equation, to study the sideband instability of Kelvin waves in superfluid helium. In this model problem, we assume that the thin vortex filament has constant cross-section.

Our numerical simulations reveal that all those methods yield qualitatively similar results. For our model problem, the self-induction equation, the Klein-Majda equation, and the Klein-Knio equation all present stable, recurrent, and chaotic phenomena, corresponding to different ratios of the amplitude of the main wave to its wavelength. The vortex filament whose motion is described by the self-induction equation, the Klein-Majda equation or the Klein-Knio equation evolves smoothly and the total arc length is almost conserved. Furthermore, hairpin structures are not formed during the vortex filament evolution . Our calculations using the self-induction equation and the Klein-Majda equation are in good agreement with the results of the linear stability theory.

The stability region of the Klein-Majda equation is closely related to the core size of the vortex filament. When the core size is larger than a critical value, the Klein-Majda equation always gives a stable solution. When the core size decreases below the critical value, the stability region of the Klein-Majda equation is smaller than that of the self-induction equation. When the core size is further decreased, the stability region of the Klein-Majda equation coincides with the stability region of the self-induction equation. For the model problem, the stability region of the Klein-Majda equation is smaller than that of

the self-induction equation.

The stability region of the Klein-Knio equation also depends on the core size of the vortex filament. The bigger the core size, the larger is the stability region. We further find that for the model problem, the Klein-Knio equation has a larger stability region than that of the self-induction equation. Hence, among our three methods for the model problem, the Klein-Knio equation gives the largest stability region, while the Klein-Majda equation has the smallest stability region.

We also carried out the computations for thicker cores with variable cross-section. A Biot-Savart model was employed. Only chaotic phenomena were observed for sideband perturbations. Our numerical results imply that thick vortices with variable cross-section may behave quite differently from thin vortices with constant cross-section. The thickness and deformation of the vortex core might play an important role in the differences between classical and superfluid vortex dynamics, which have been highlighted by Buttke [11].

In the derivations of the self-induction equation, the Klein-Majda equation, and the Klein-Knio equation, we have assumed a thin model, in which hairpins [24] are excluded; our numerical results have no hairpins, and therefore the slender model is self-consistent, at least for a class of problems that contains our model problem. Since the models are increasingly refined (i.e the Klein-Knio model takes more effects into account than the Klein-Majda model, which in turn is a more accurate approximation than the self-induction equation), it is reasonable to conjecture that motion without hairpins is self-consistent for a class of thin vortex filaments of small-enough cross-section.

If one views superfluid vortices as very thin constant cross-section classical vortices,

the conclusion is consistent with the statistical theory of vortex motion [7] which shows that classical vortices, with finite and deformable cross-section, have a temperature determined by vortex stretching, while superfluid vortex systems have a constant temperature determined by boundary conditions.

The difference between classical and quantum vortices are often explained as a consequence of quantization; according to our results, maybe slenderness is even more important. Of course, only very slender vortices can have a quantized circulation.

If the self-induction equation, the Klein-Majda equation, and the Klein-Knio equation are used to describe superfluid turbulence [11],[25],[26], then the physical assumption that there is no vortex folding on small scale has been implicitly made. Our numerical simulations suggest that this may be a reasonable conclusion for a single filament, but is for the moment an additional assumption for a tangle of filaments. Deeper understanding remains to be found.

7 Acknowledgements

This work is based in part on the author's Ph.D. dissertation, carried out under the supervision of Prof. Alexandre Chorin. It was supported in part by the Applied Mathematical Sciences Subprogram of the Office of Energy Research, U.S. Department of Energy under Contract DE-AC03-76SF00098. All computations were performed at the Lawrence Berkeley National Laboratory.

References

[1] G. K. Batchelor, *An introduction to fluid mechanics* (Cambridge University Press, Cambridge, 1967).

[2] R. Klein and A. Majda, "Self-stretching of a perturbed vortex filament (I)," Physica D **49**, 323 (1991).

[3] R. Klein and O. M. Knio, "Asymptotic vorticity structure and numerical simulation of slender vortex filaments," J. Fluid Mech. **284**, 275 (1995).

[4] A. J. Chorin and J. Akao, "Vortex equilibria in turbulence theory and quantum analogues," Physica D **51**, 403 (1991).

[5] A. Majda, "Vorticity, turbulence, and acoustics in fluid flow," SIAM Rev. **33**, 349 (1991).

[6] A. J. Chorin, "Turbulence and vortex stretching on a lattice," Commun. on Pure and Applied Math. **XXXIX**, S47 (1986).

[7] A. J. Chorin, *Vorticity and Turbulence* (Springer, 1993).

[8] A. J. Chorin, "Vortex phase transitions in 2.5 dimensions," J. Stat. Phys. **76**, 835 (1994).

[9] A. J. Chorin and O. Hald, "Vortex renormalization in three space dimensions," Physical Review B **51**, 11969 (1995).

[10] S. E. Widnall, D. B. Bliss and C. Y. Tsai, "The instability of short waves on a vortex ring," J. Fluid Mech. **66**, 35 (1974).

[11] T. F. Buttke, "Numerical study of superfluid turbulence in the self-induction approximation," J. Comput. Phys. **76**,301 (1988).

[12] H.Hasimoto, "A soliton on a vortex filament," J. Fluid Mech. **51**, 477 (1972).

[13] R. Klein and A. Majda, "Self-stretching of perturbed vortex filaments (II): Structure of solutions," Physica D **53**, 267 (1991).

[14] O. M. Knio and A. F. Ghoniem, "Numerical study of a three-dimensional vortex method," J. Comput. Phys. **86**, 75 (1990).

[15] J. T. Beale and A. Majda, "High order accurate vortex methods with explicit velocity kernals," J. Comput. Phys. **58**, 188 (1985).

[16] T. F. Buttke, "A numerical study of superfluid turbulence in the self-induction approximation," Ph.D thesis, University of California, Berkeley, 1986.

[17] P. J. Prince and J. R. Dormand, "High order embedded Runge-Kutta formulae," J. Comput. and Appl. Math. **7**, 67 (1981).

[18] T. B. Benjamin and J. E. Feir, "The disintegration of wave trains on deep water," J. Fluid Mech. **27**, 417(1967).

[19] H. C. Yuen and W. E. Ferguson, Jr. "Relationship between Benjamin-Feir instability and recurrence in the nonlinear Schrödinger equation," Phys. Fluids, **21**, 1275(1978).

[20] D. R. Andersen, S. Datta and R. J. Gunshor, " A coupled mode approach to modulation instability and envelope solitons," J. Appl. Phys. **54**, 5608(1983).

[21] D. C. Samuels and R. J. Donnelly, "Sideband instability and recurrence of Kelvin waves on vortex core," Phys. Rev. Lett. **64**, 1385 (1990).

[22] E. Fermi, S. Ulam and J. Pasta, "Studies on non linear problems", in *Collected papers of Enrico Fermi II* edited by E. Segré (University of Chicago, 1965).

[23] A. J. Chorin, " Vortex Methods," Les Houches Summer School of Theoret. Phys. **59** (1995).

[24] A. J. Chorin, "Hairpin removal in vortex interactions," J. Comput. Phys. **91**, 1(1990).

[25] R. J. Donnelly, "Quantized Vortices in Helium II," Ann. Rev. Fluid Mech. **25**, 325(1993).

[26] K. W. Schwarz, "Generation of superfluid turbulence deduced from simple dynamical rules," Phys. Rev. Lett. **49**, 283(1982).

List of Figures

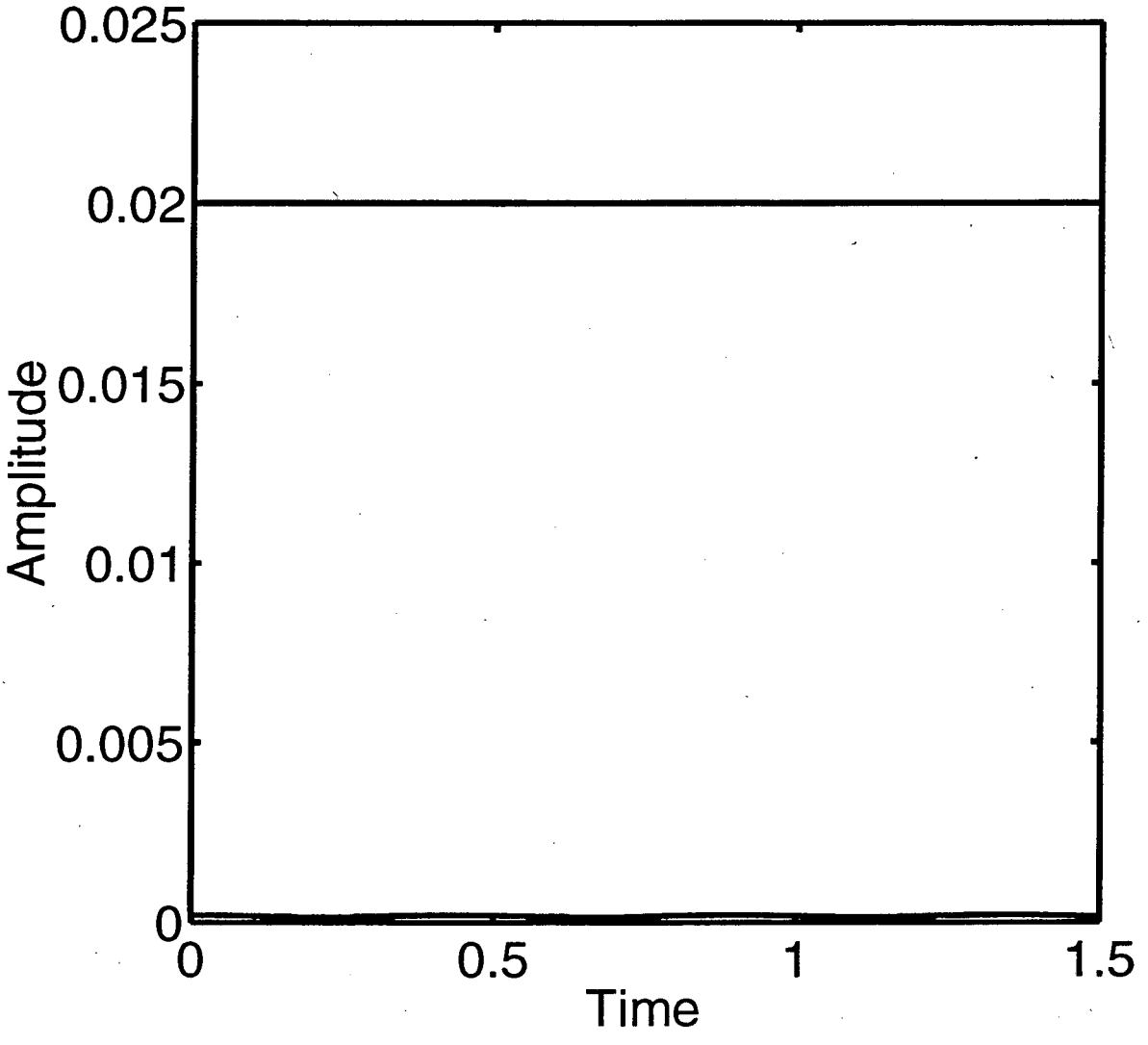

Figure 1 (a)

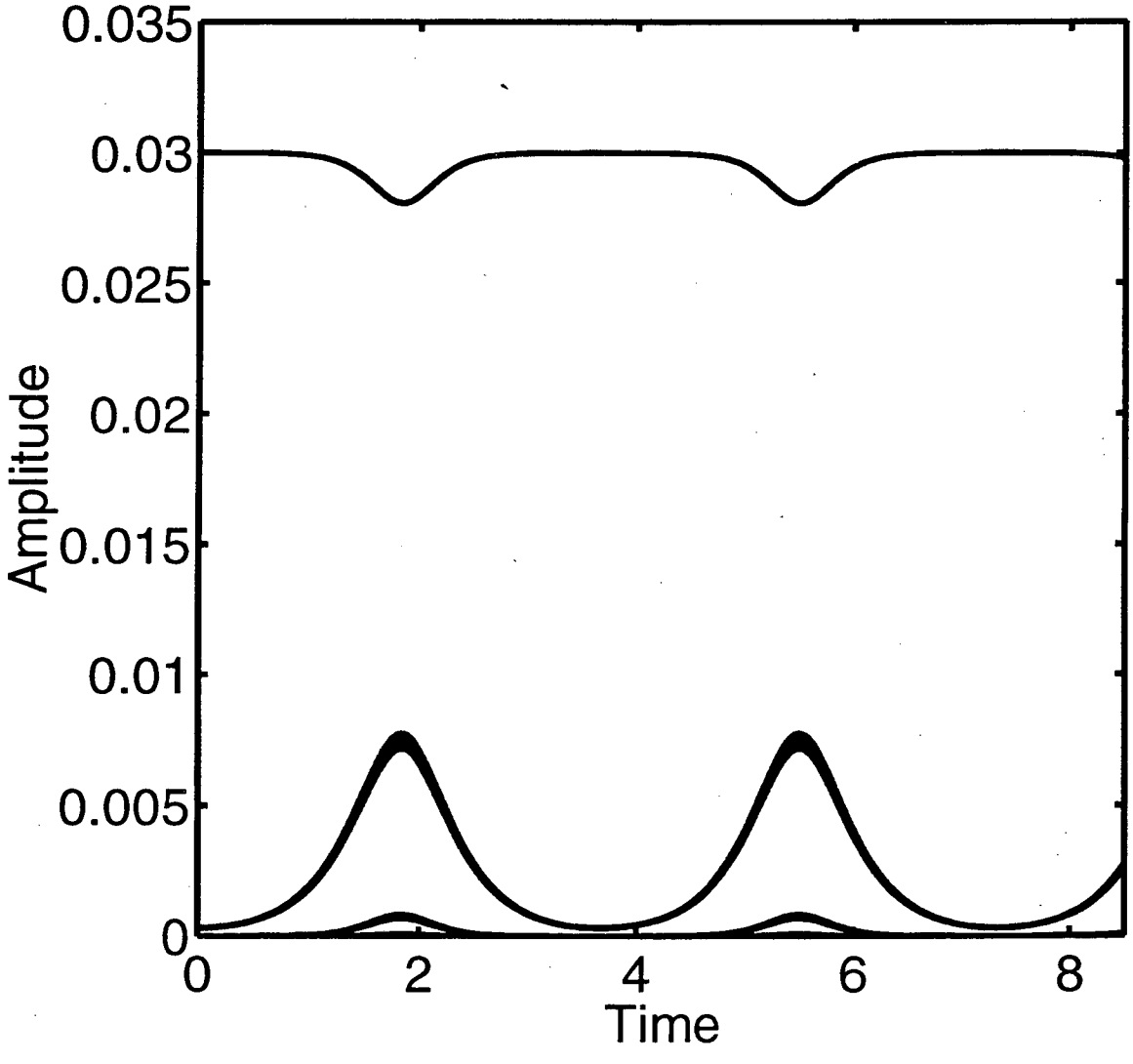

Figure 1 (b)

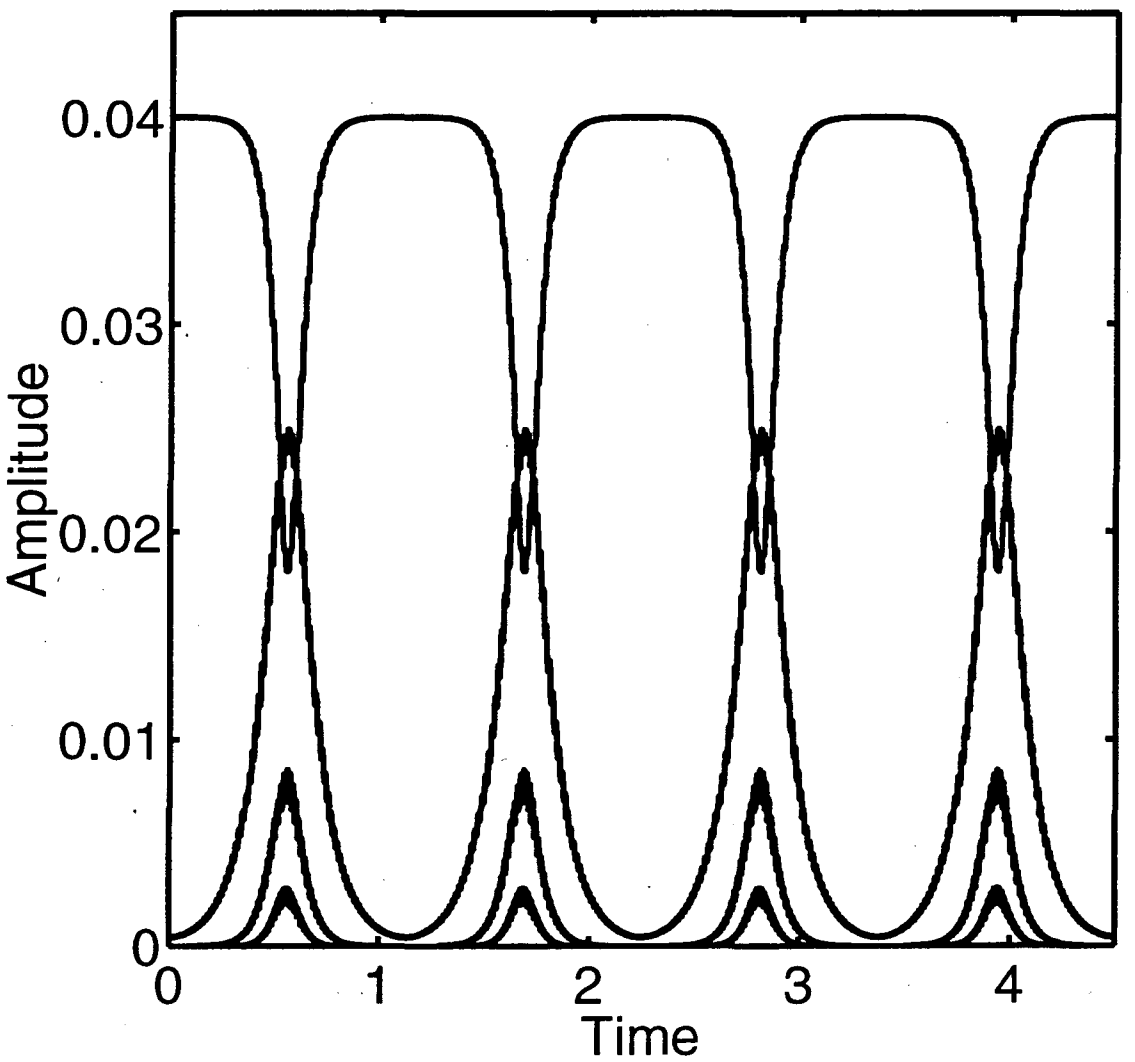

Figure 1 (c)

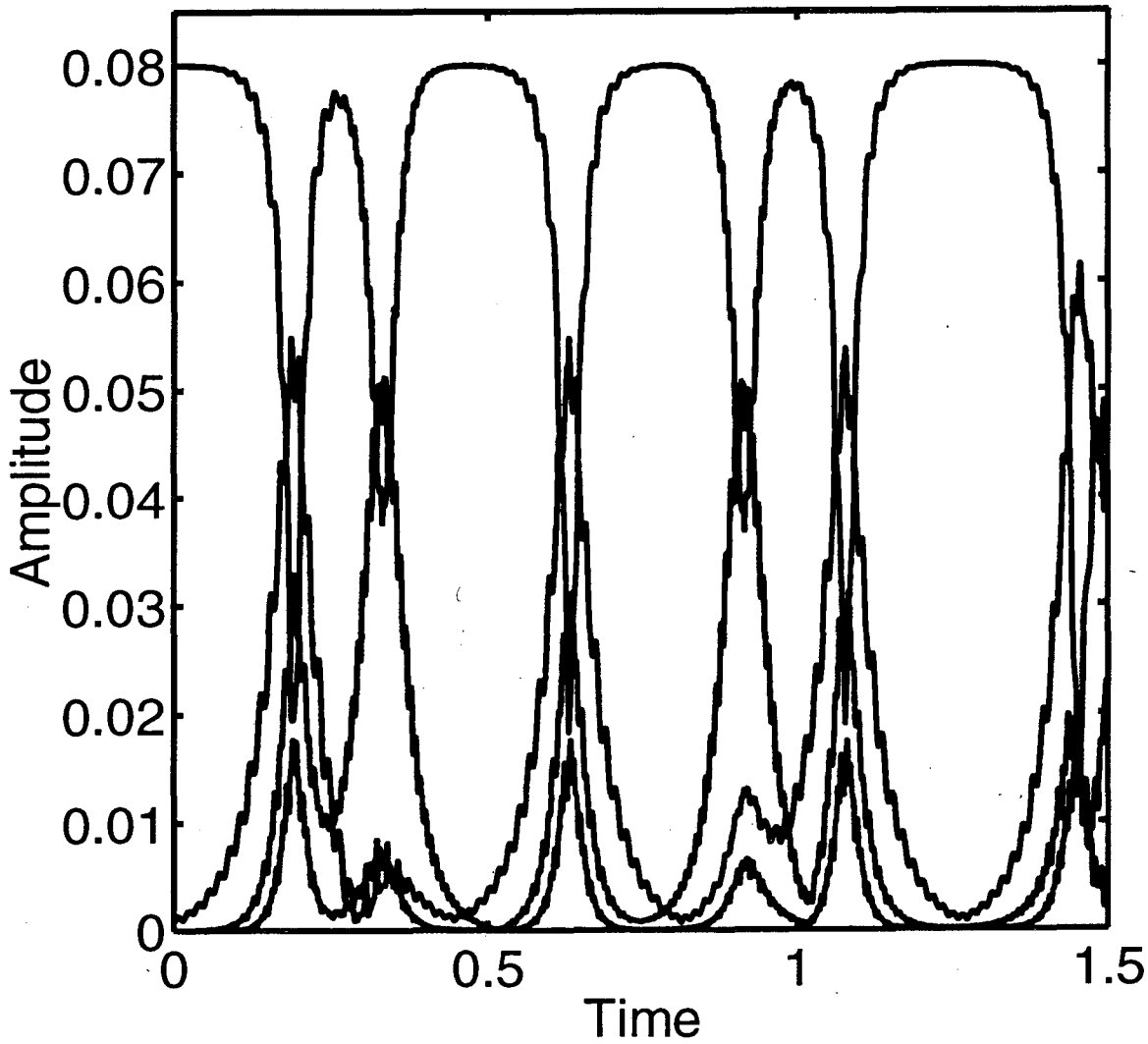

Figure 1 (d)

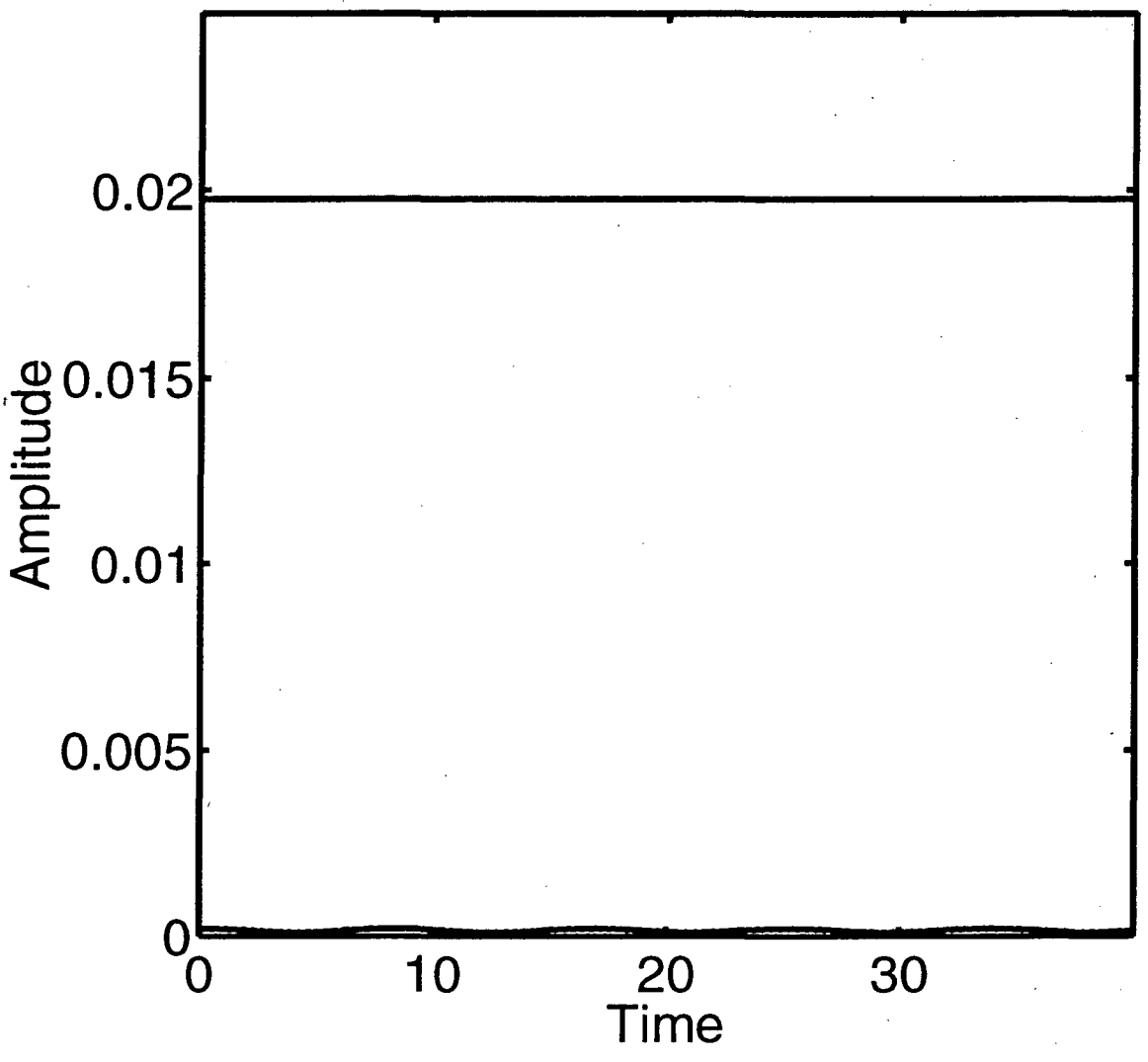

Figure 2 (a)

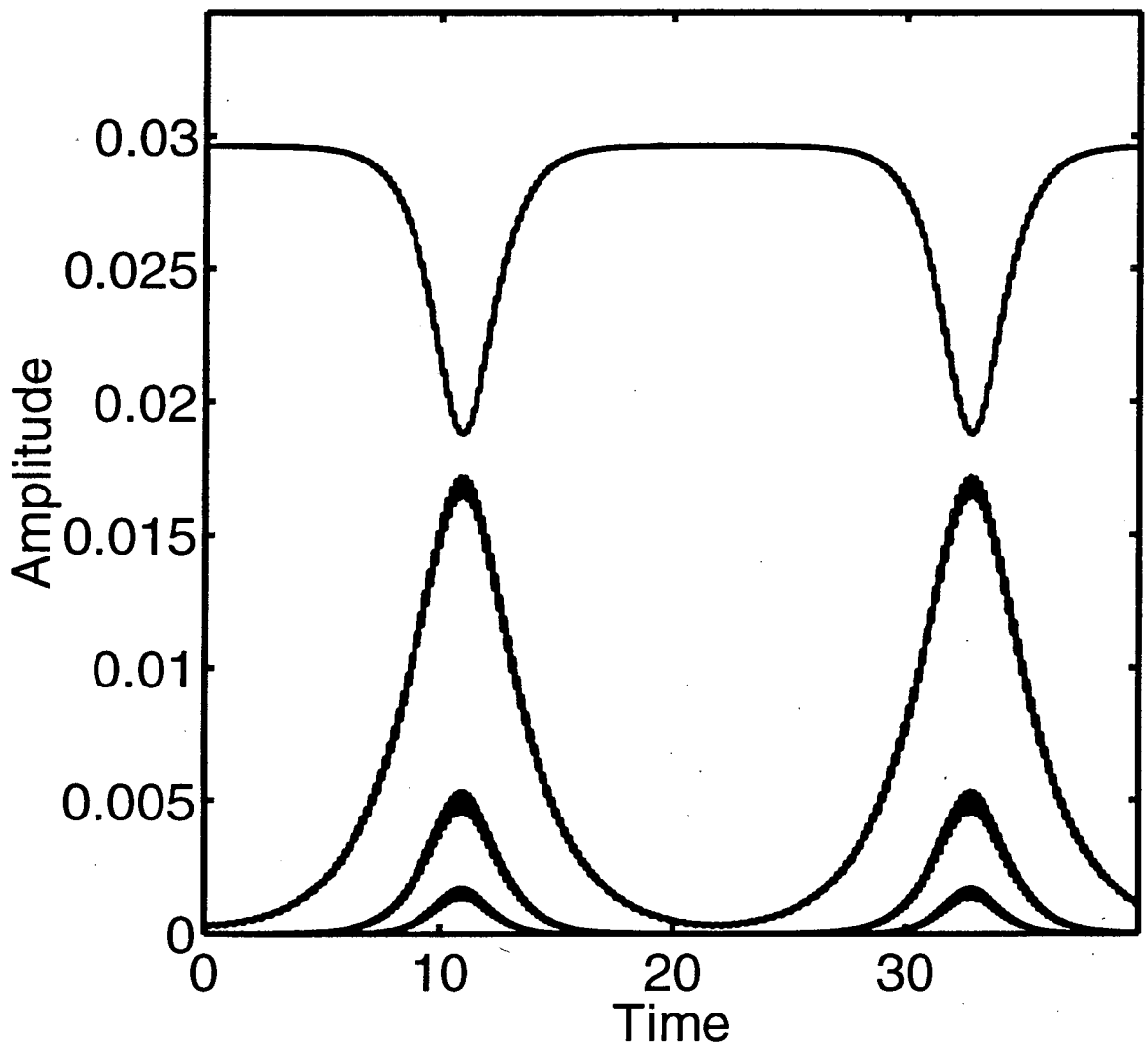

Figure 2 (b)

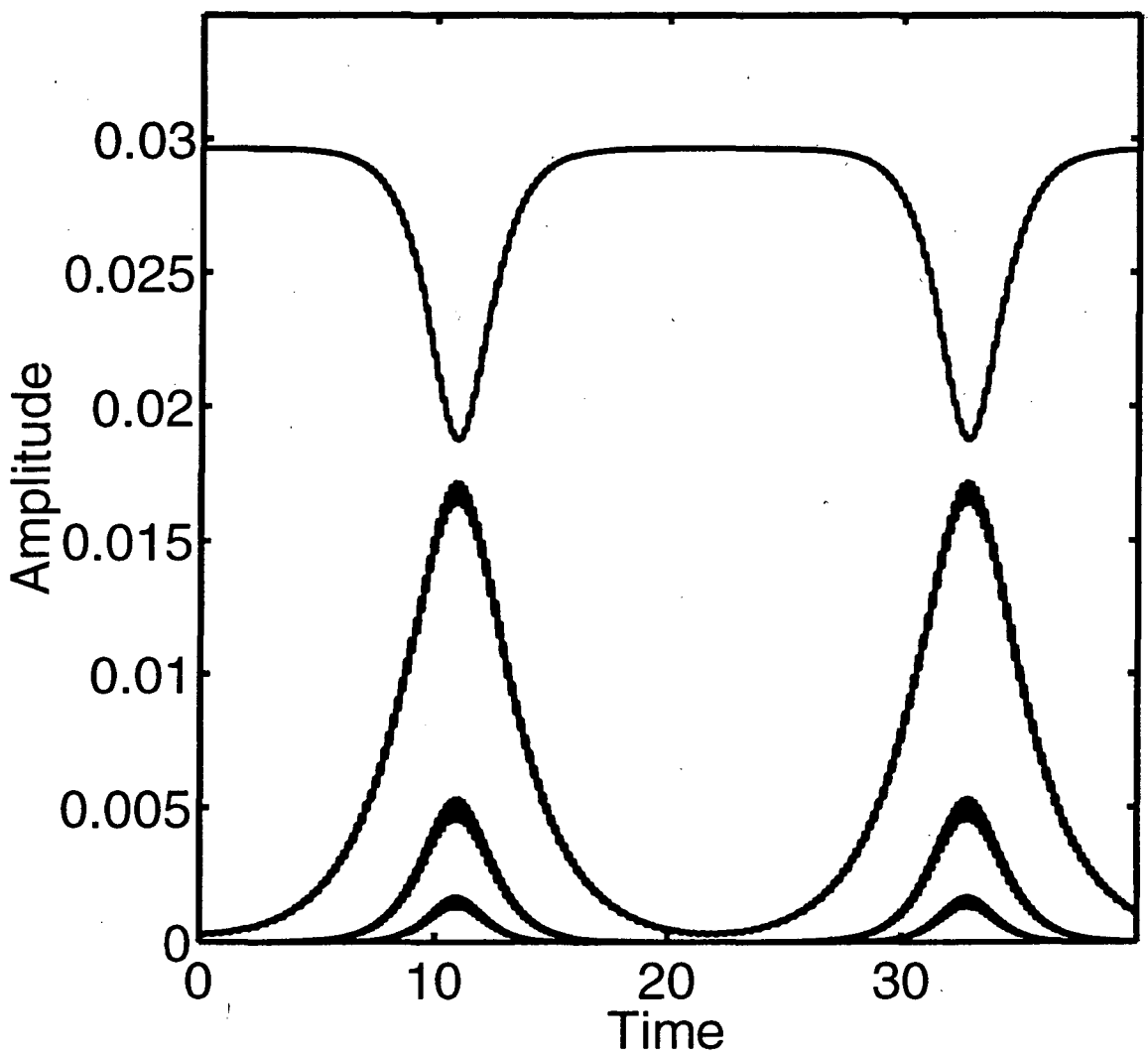

Figure 2 (c)

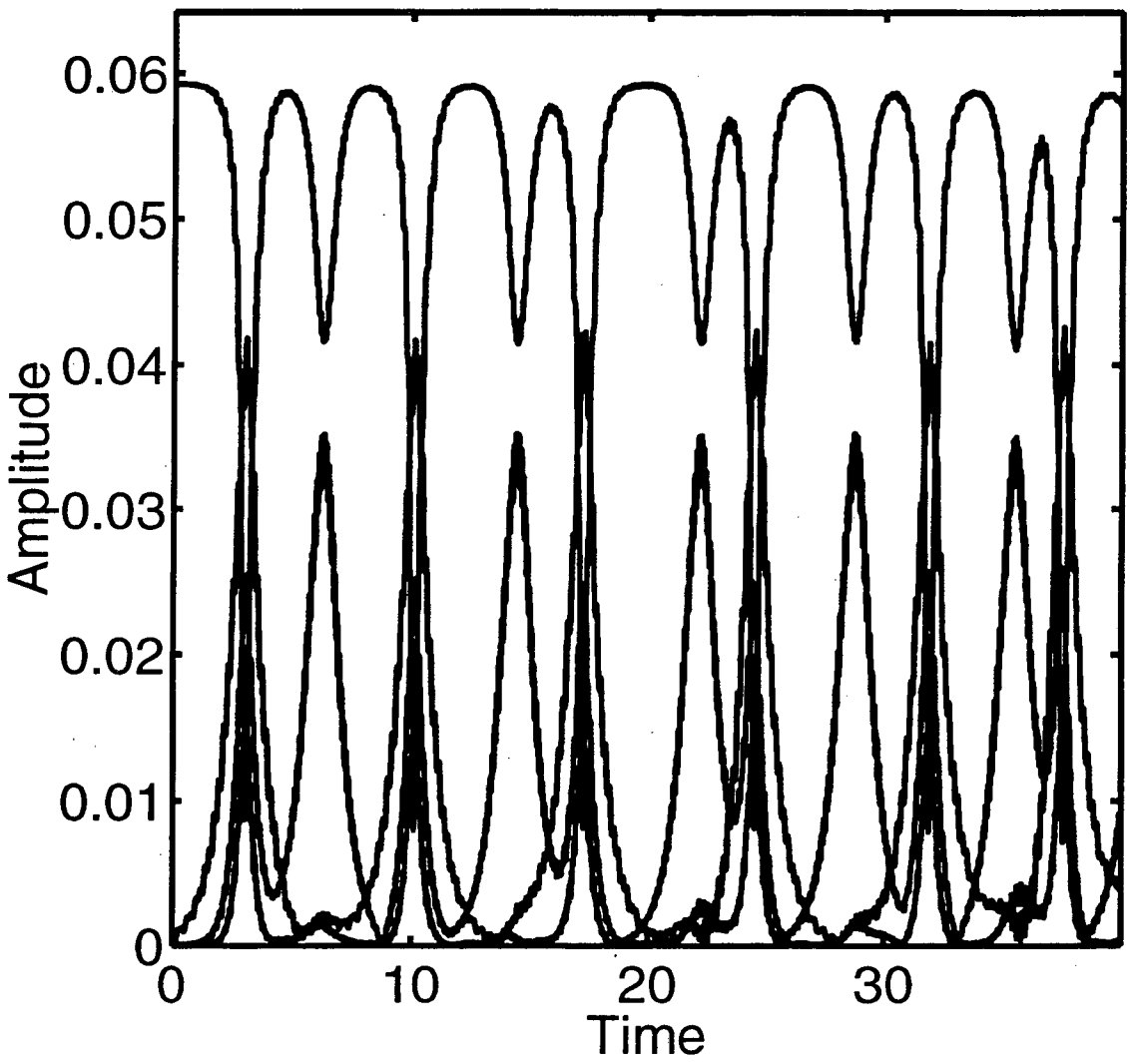

Figure 2 (d)

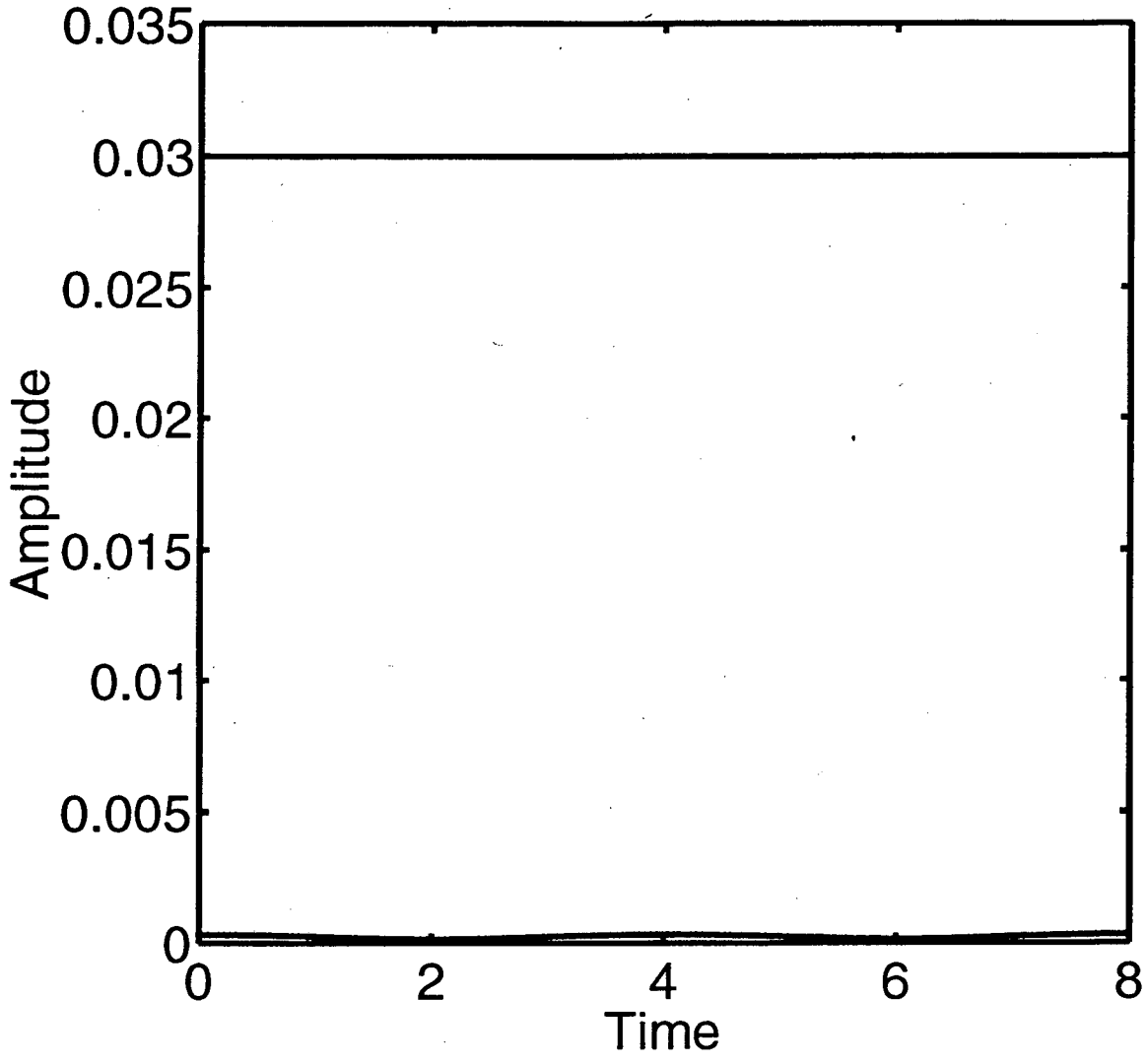

Figure 3 (a)

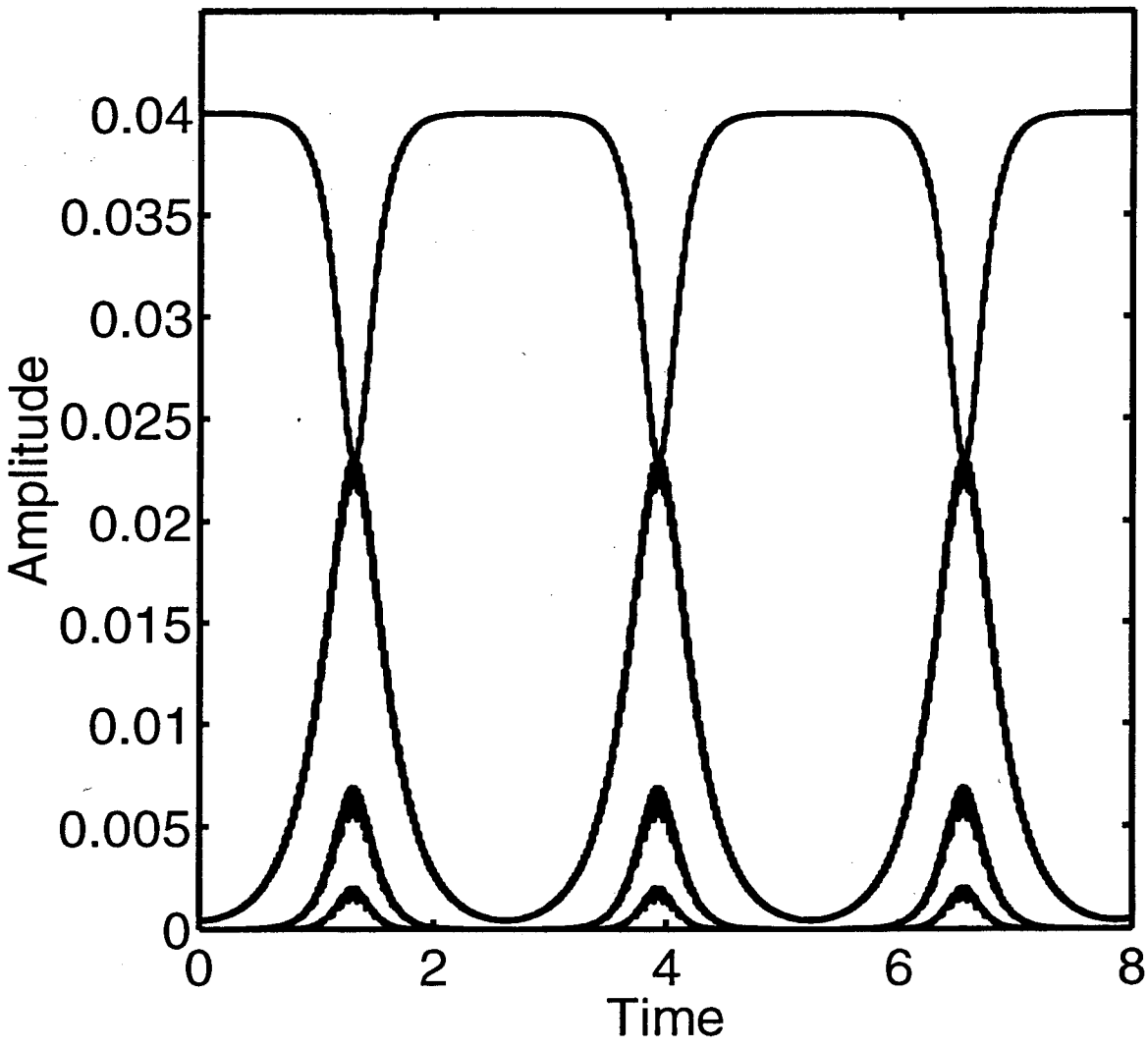

Figure 3 (b)

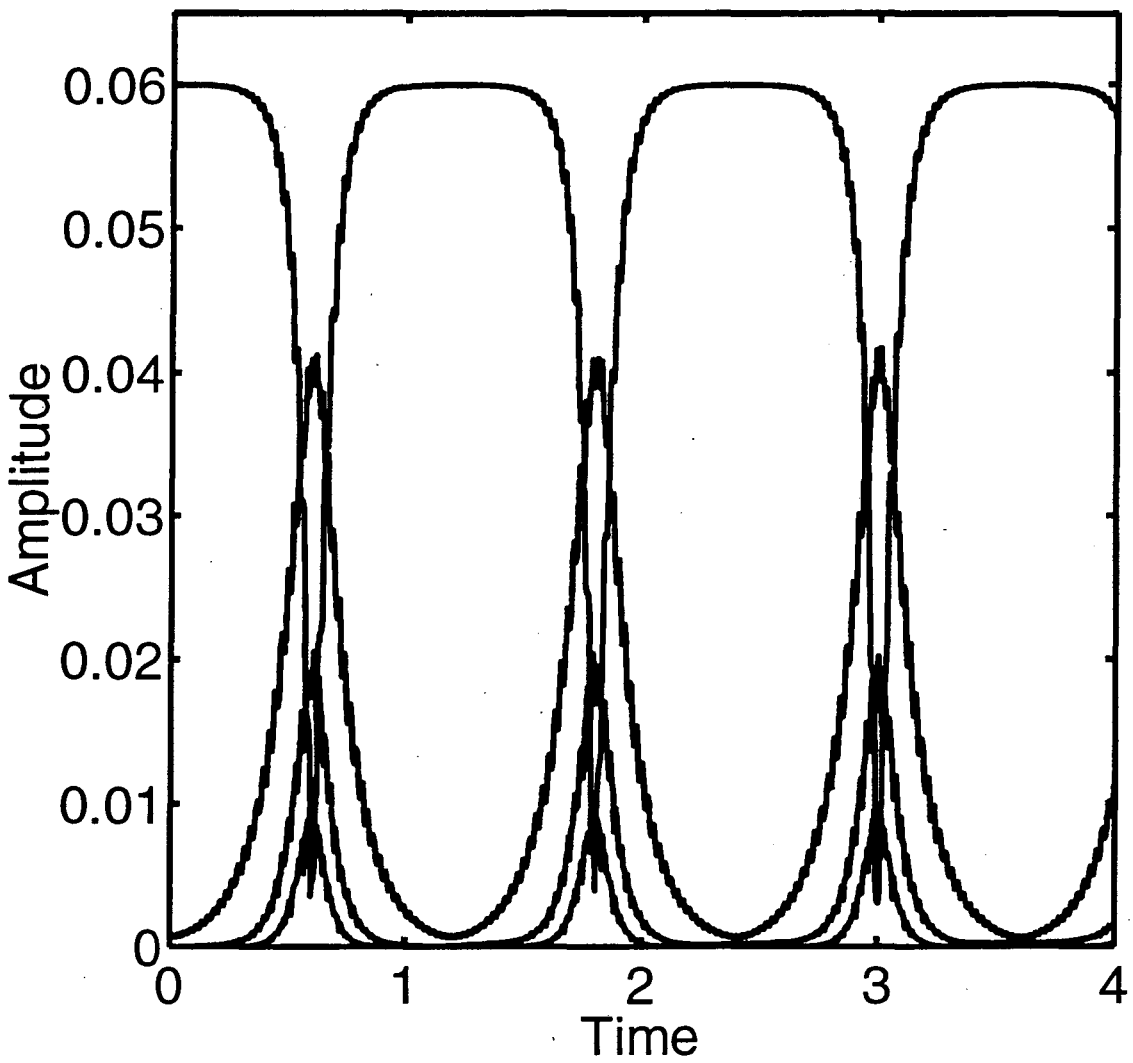

Figure 3 (c)

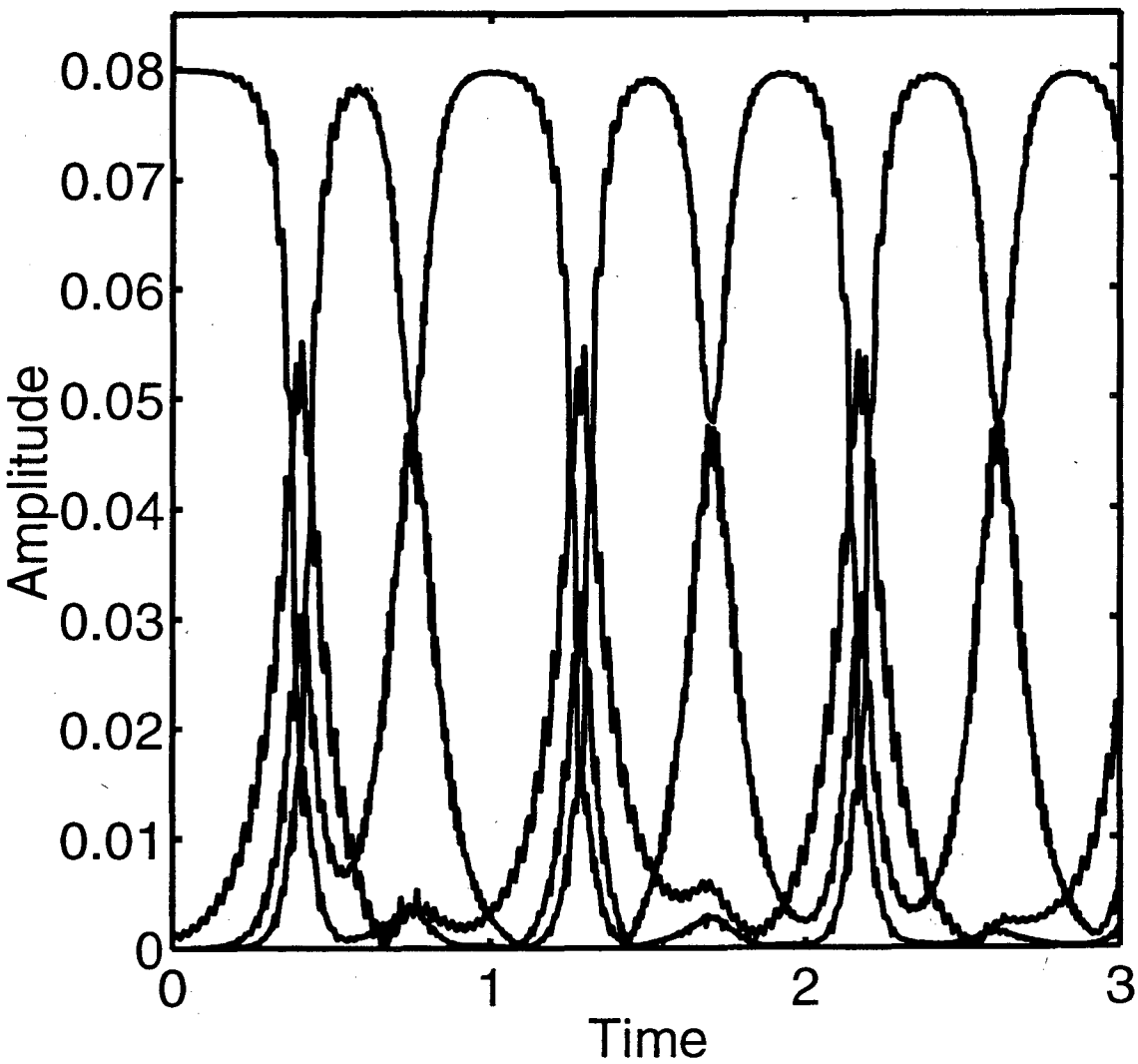

Figure 3 (d)

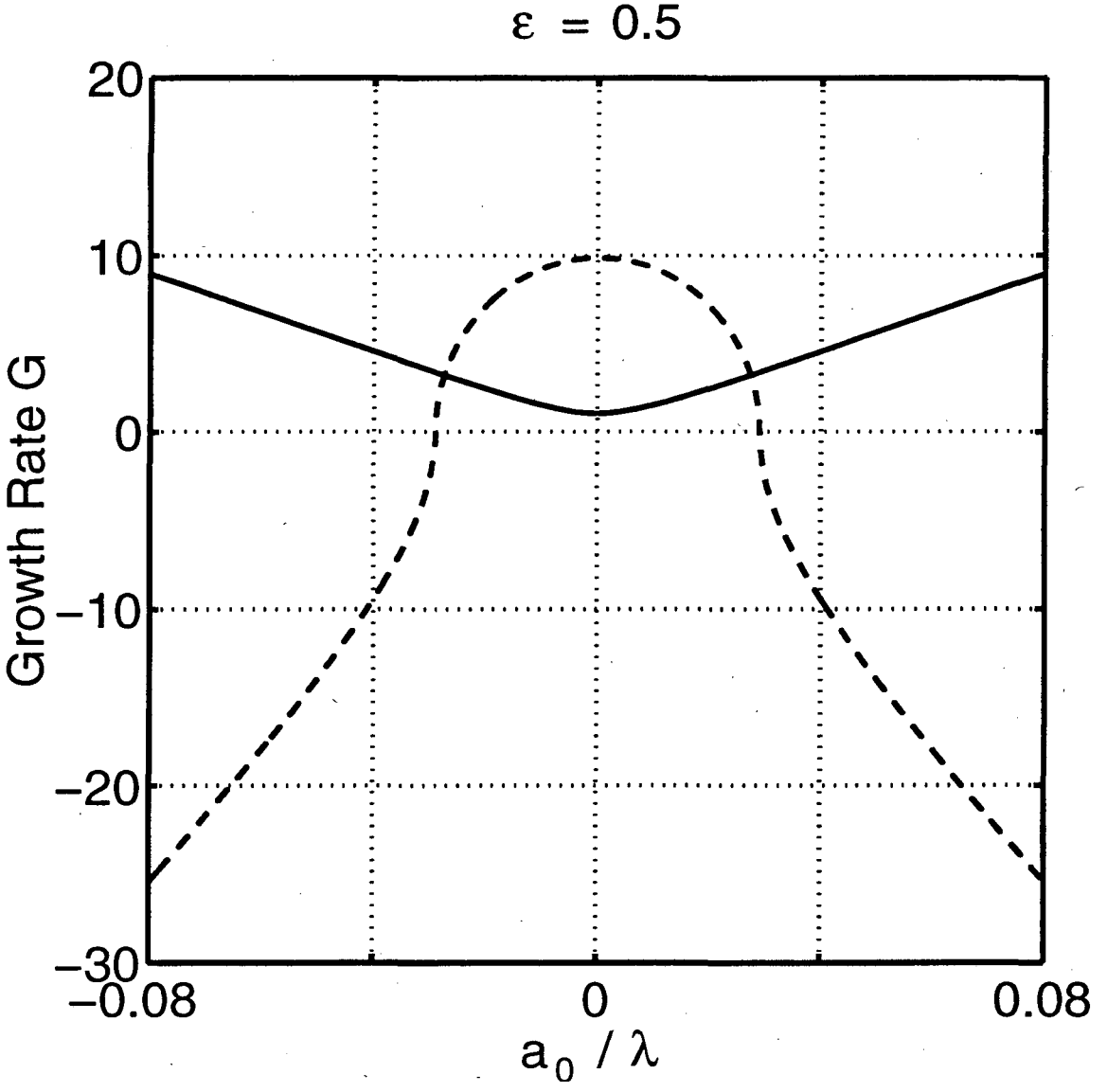

Figure 4 (a)

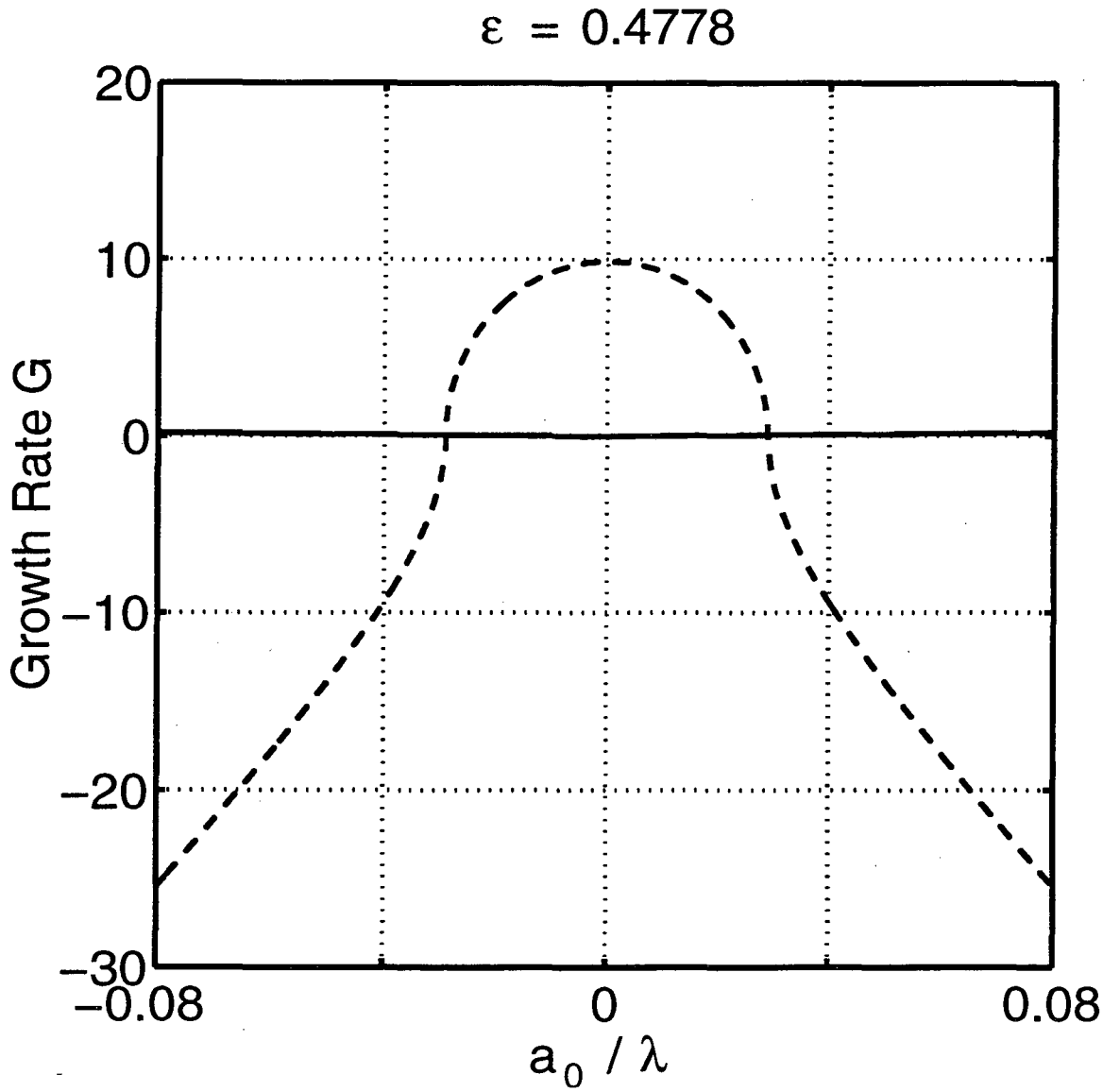

Figure 4 (b)

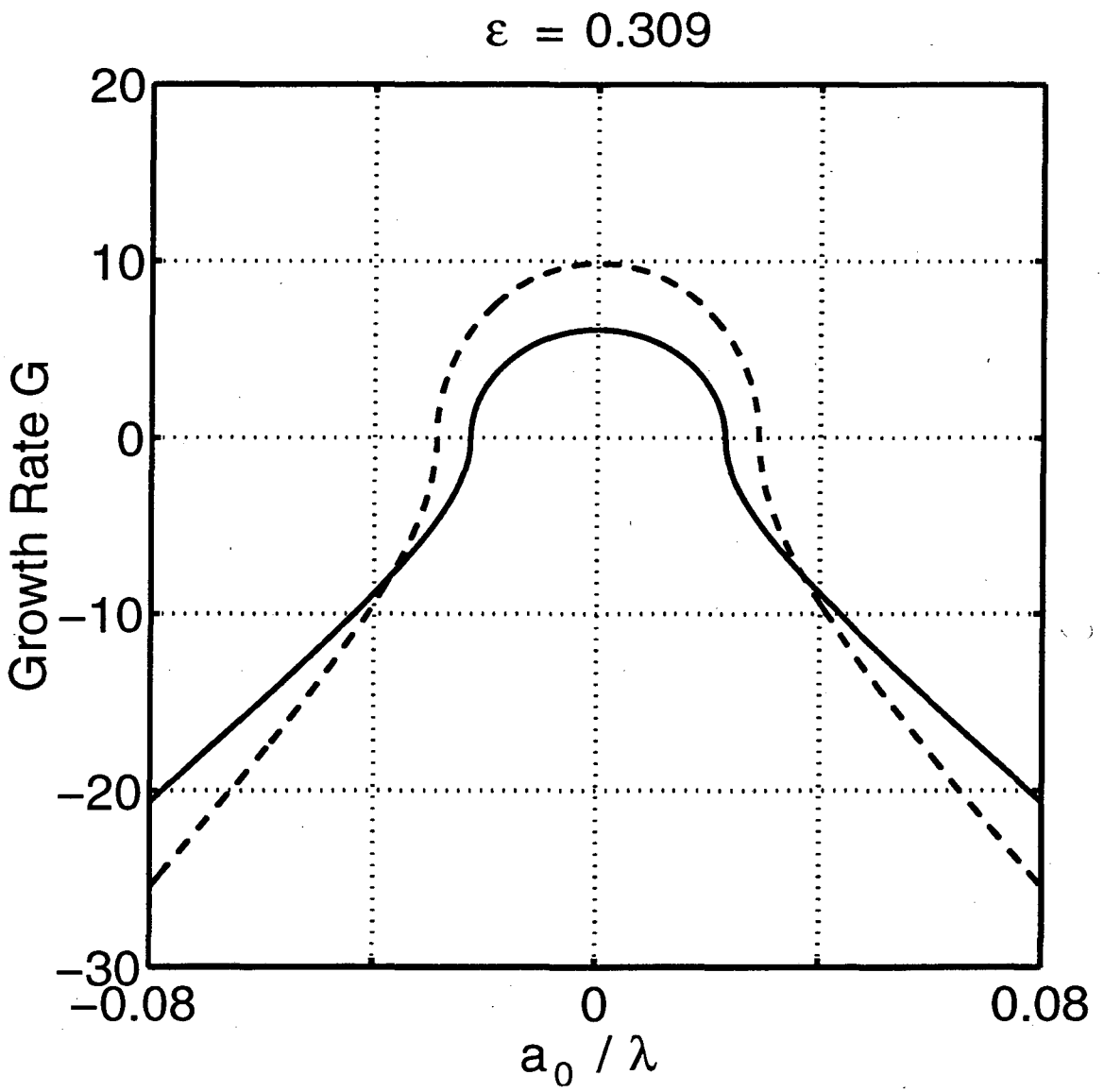

Figure 4 (c)

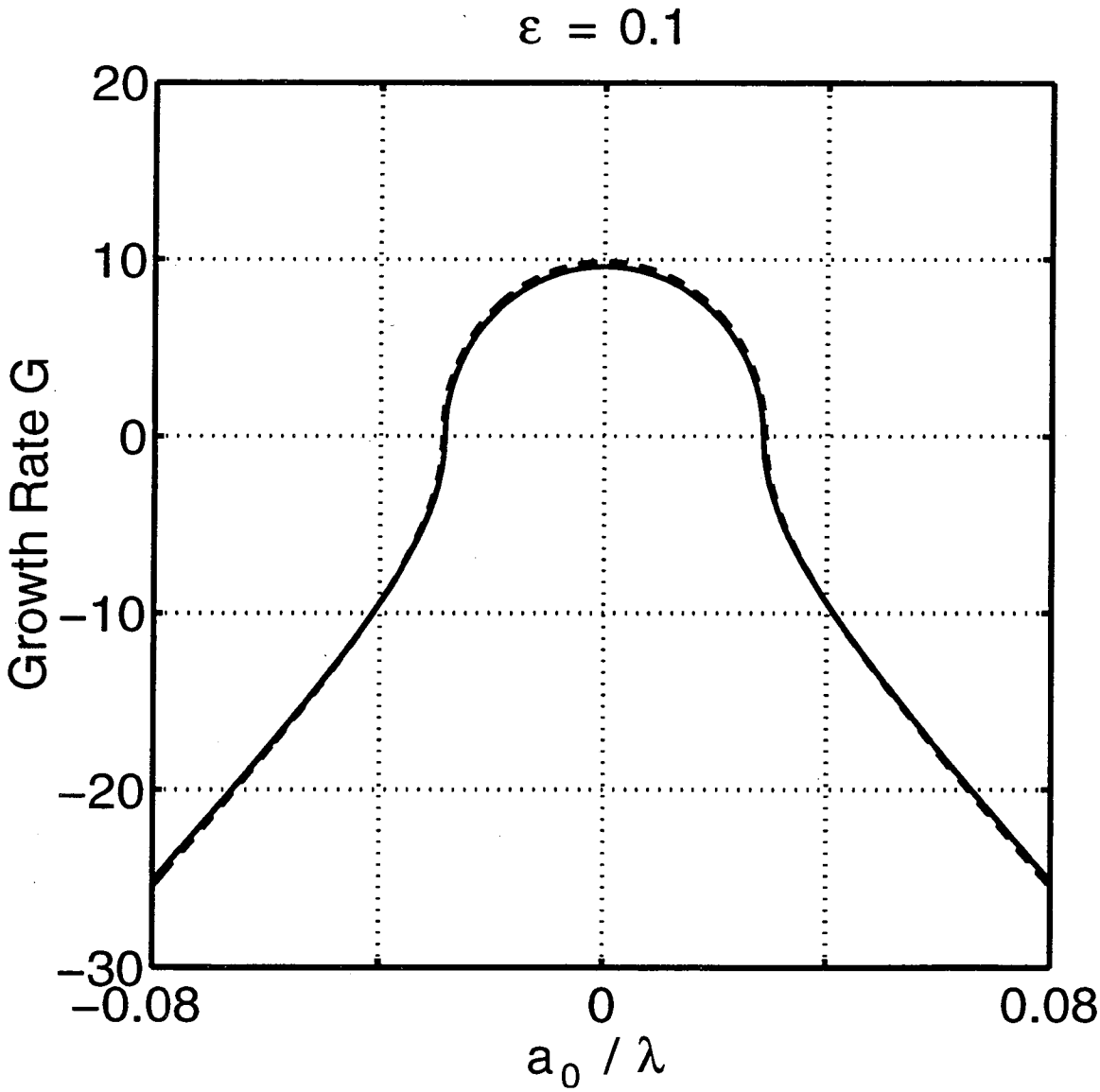

Figure 4 (d)

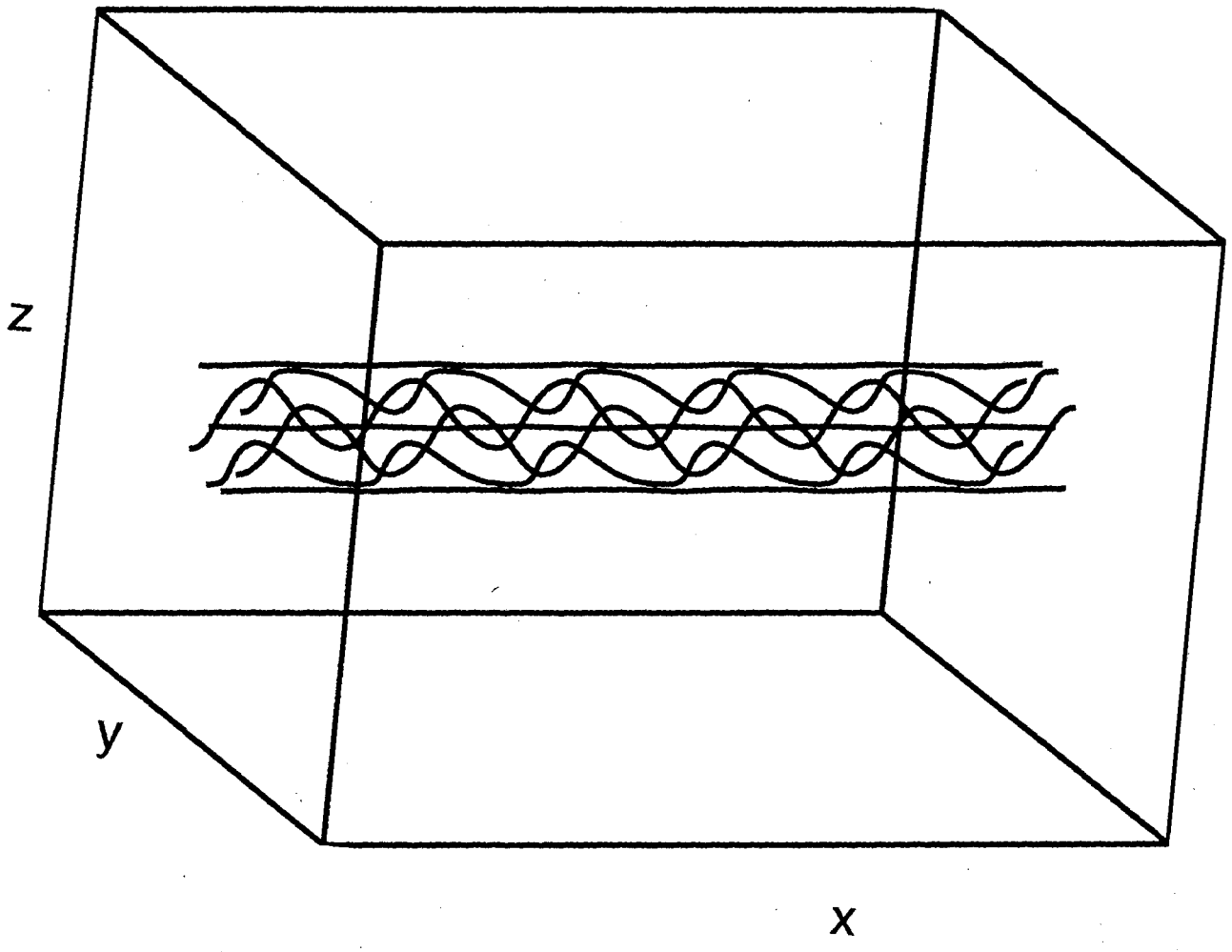

Figure 5 (a)

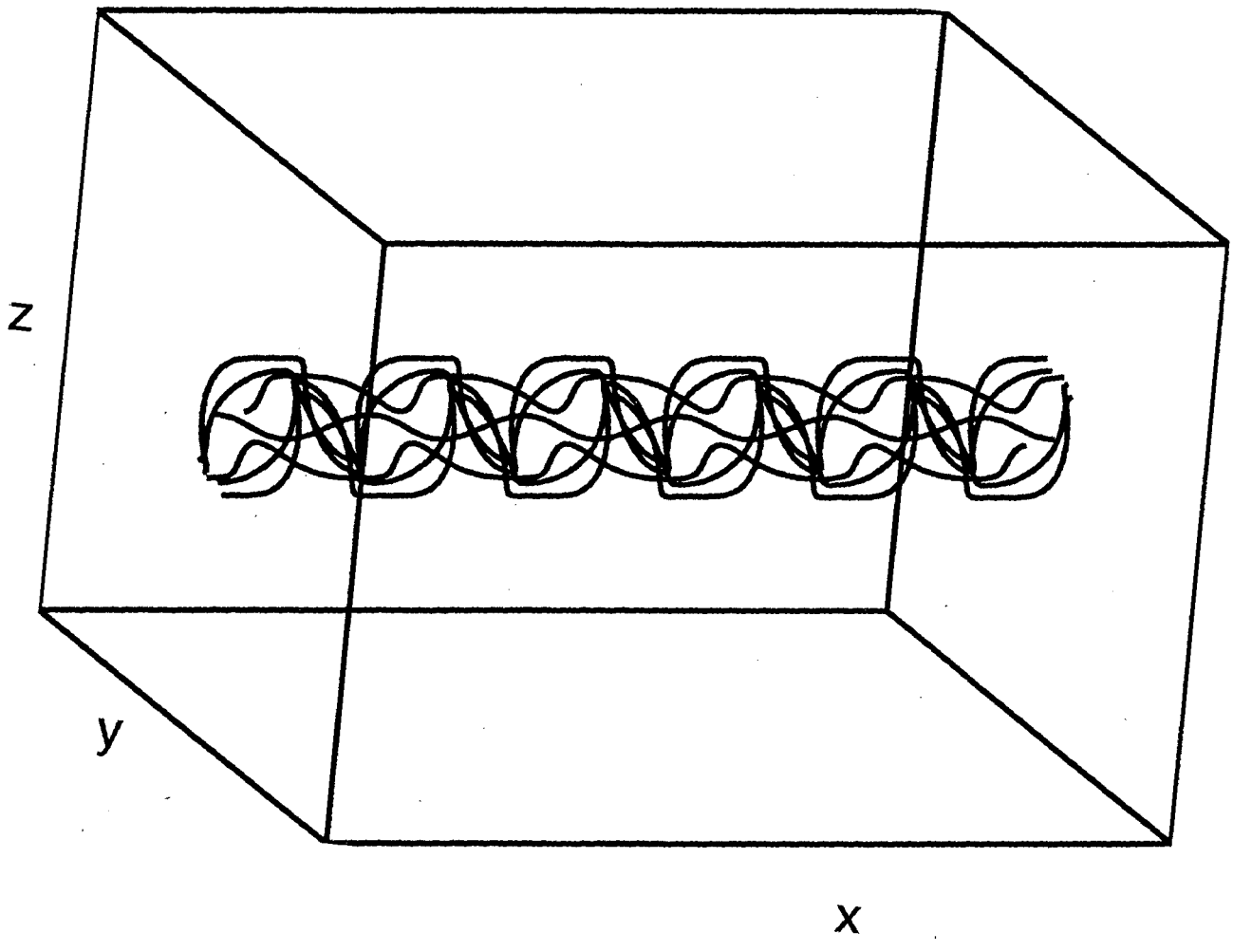

Figure 5 (b)

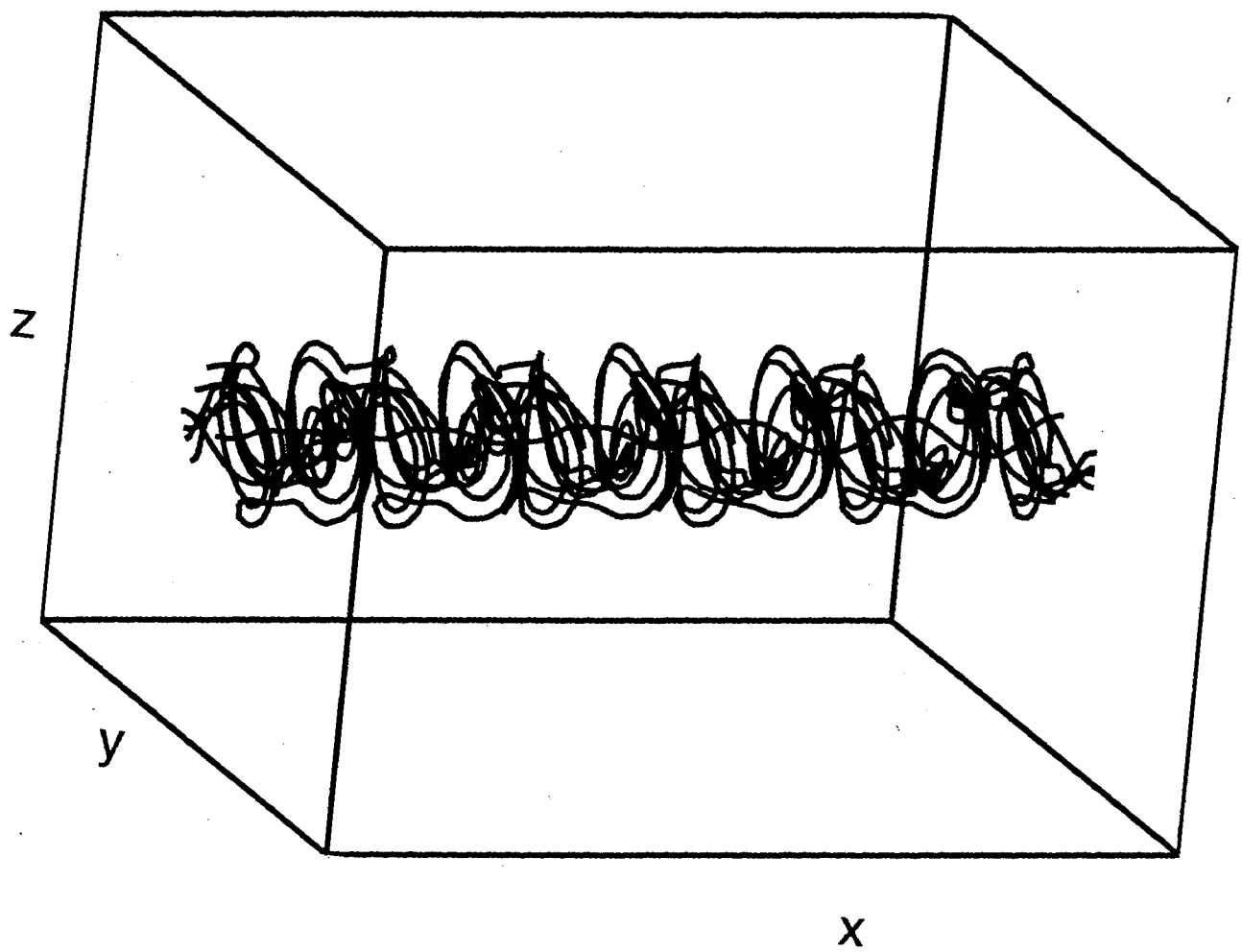

Figure 5 (c)

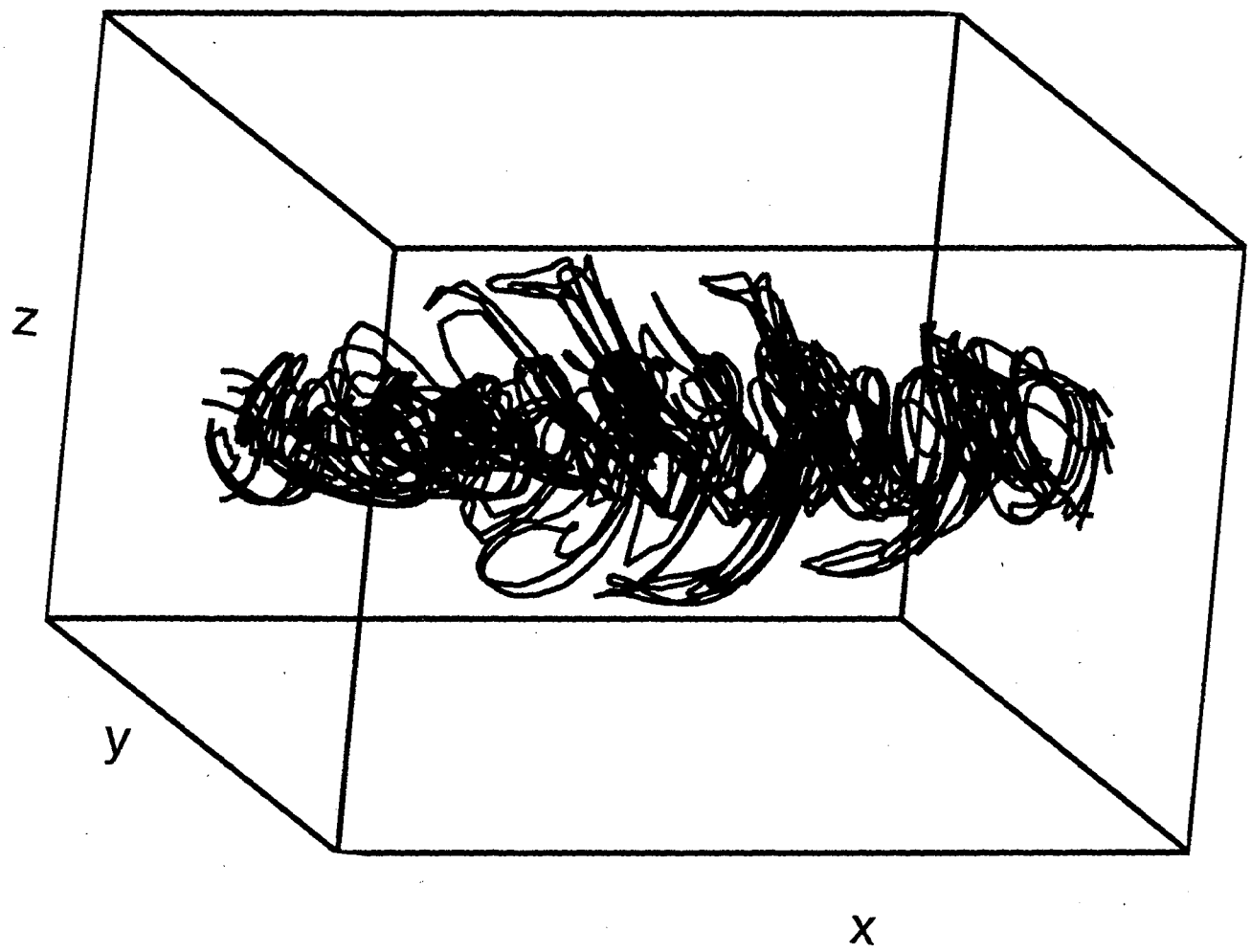

Figure 5 (d)

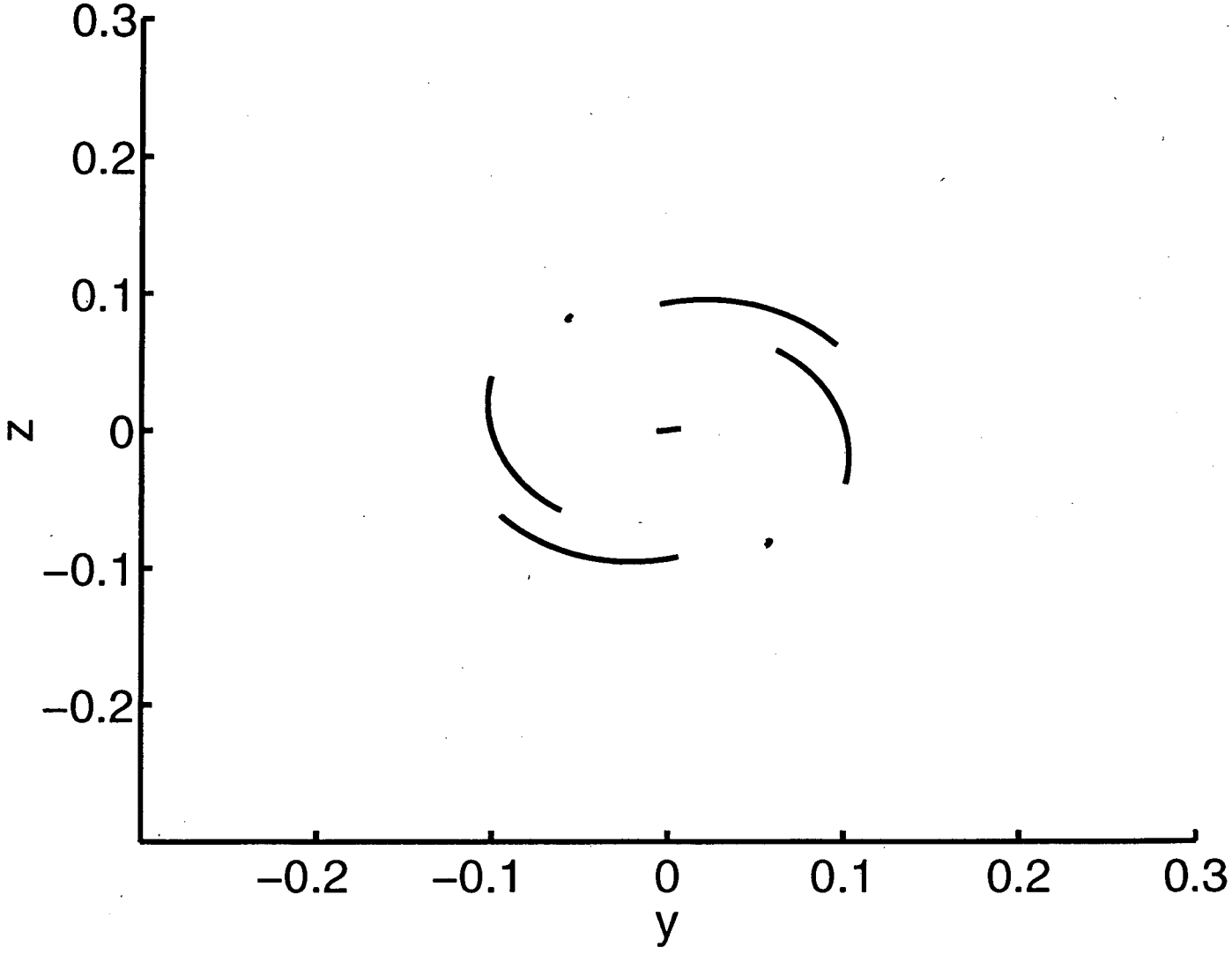

Figure 6 (a)

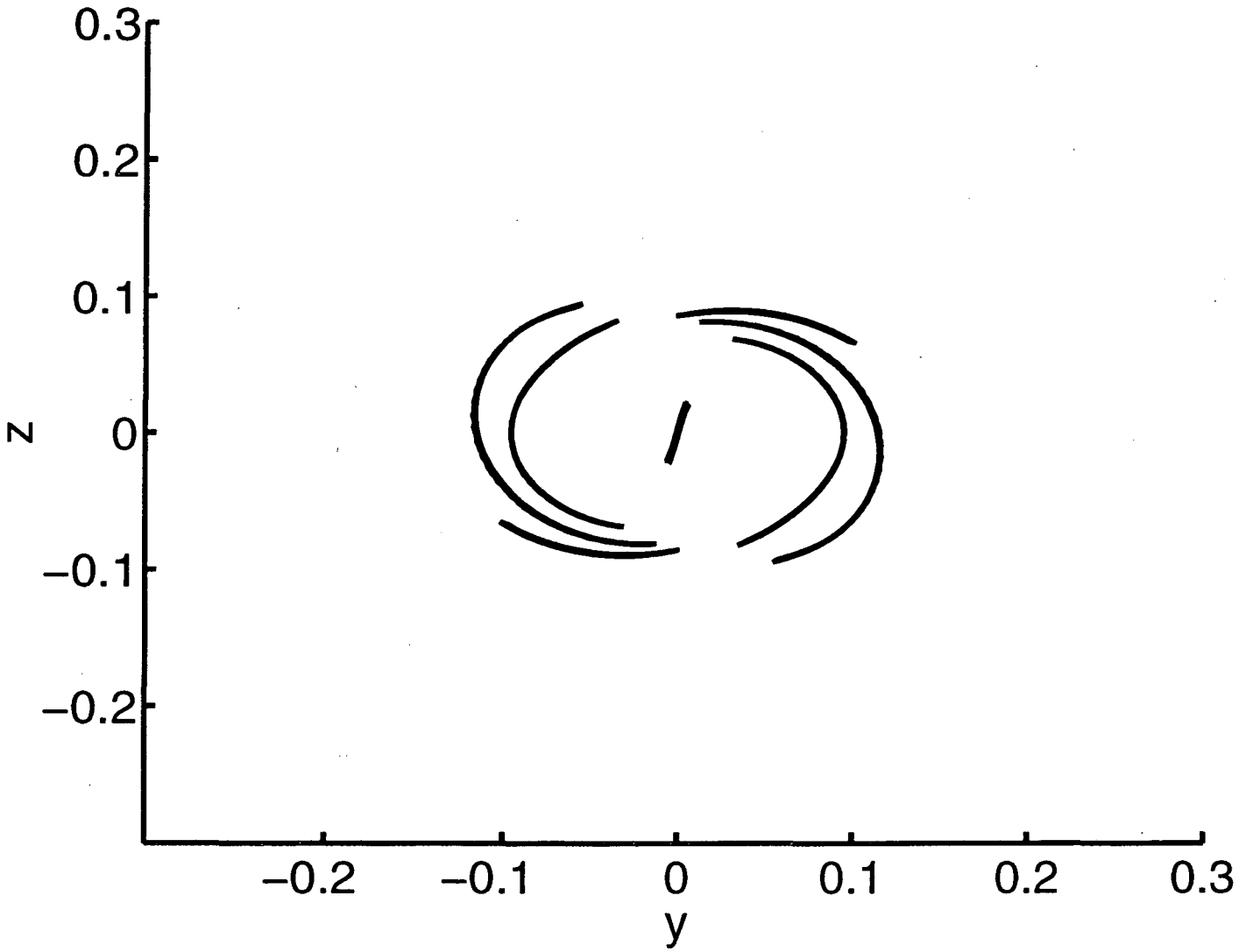

Figure 6 (b)

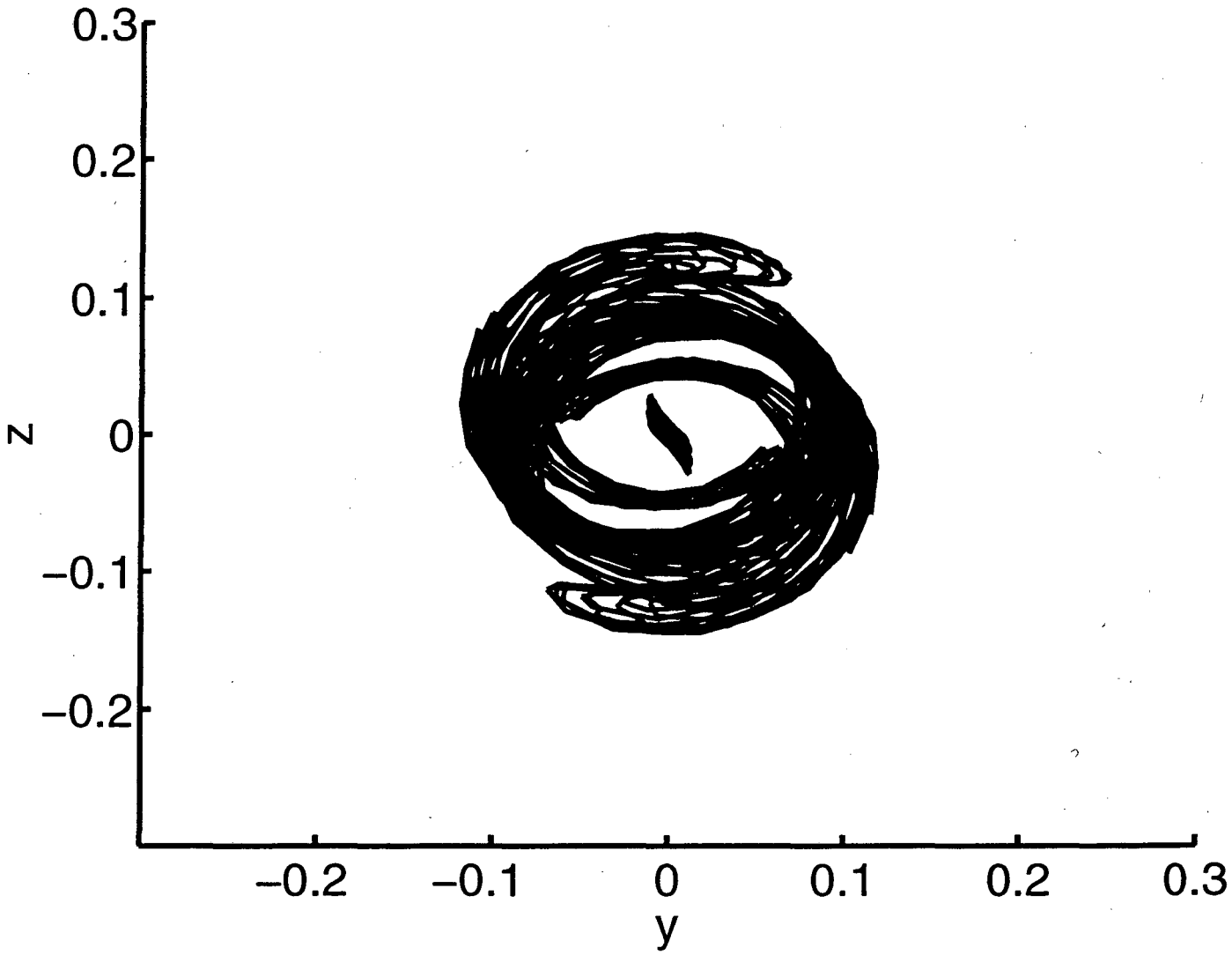

Figure 6 (c)

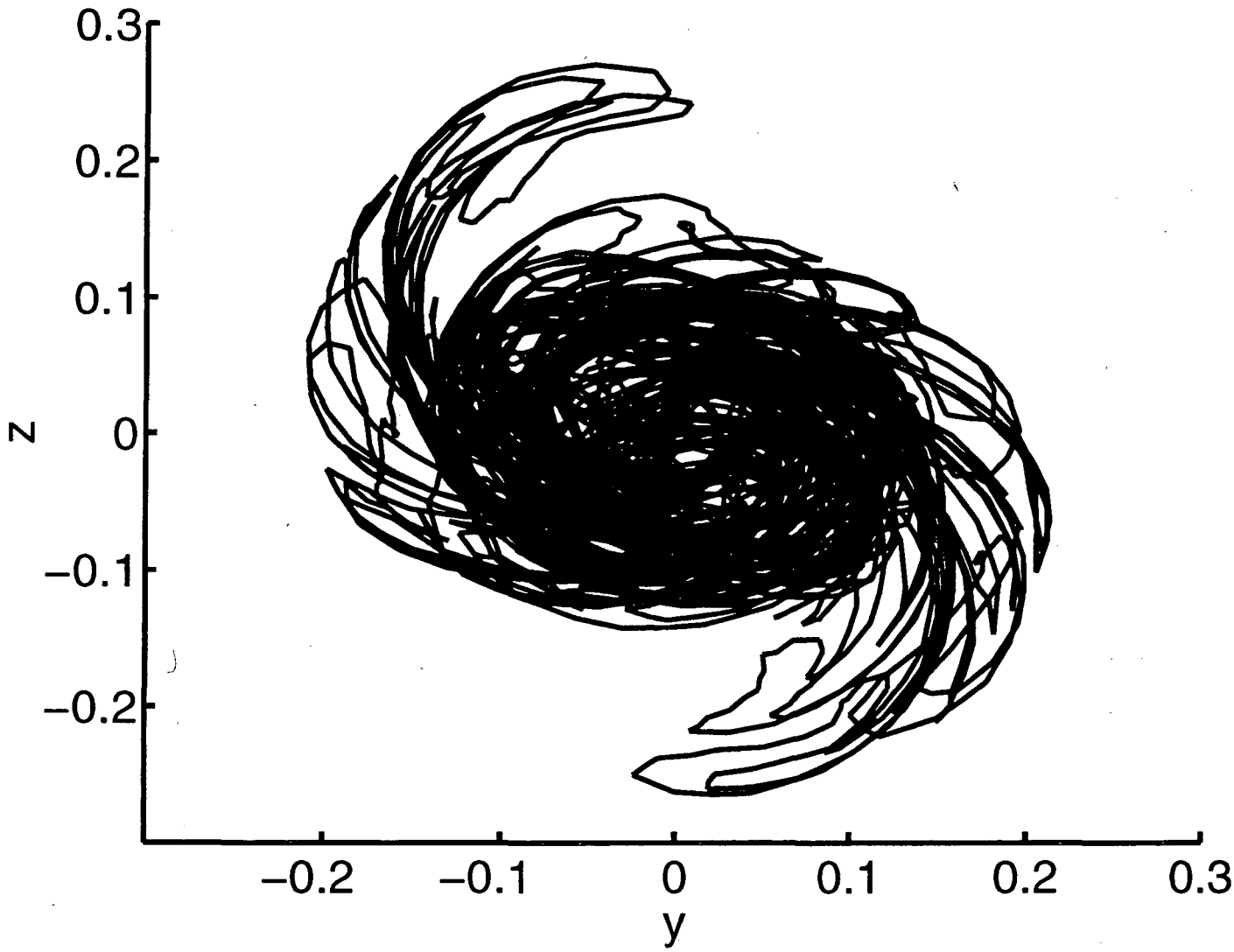

Figure 6 (d)

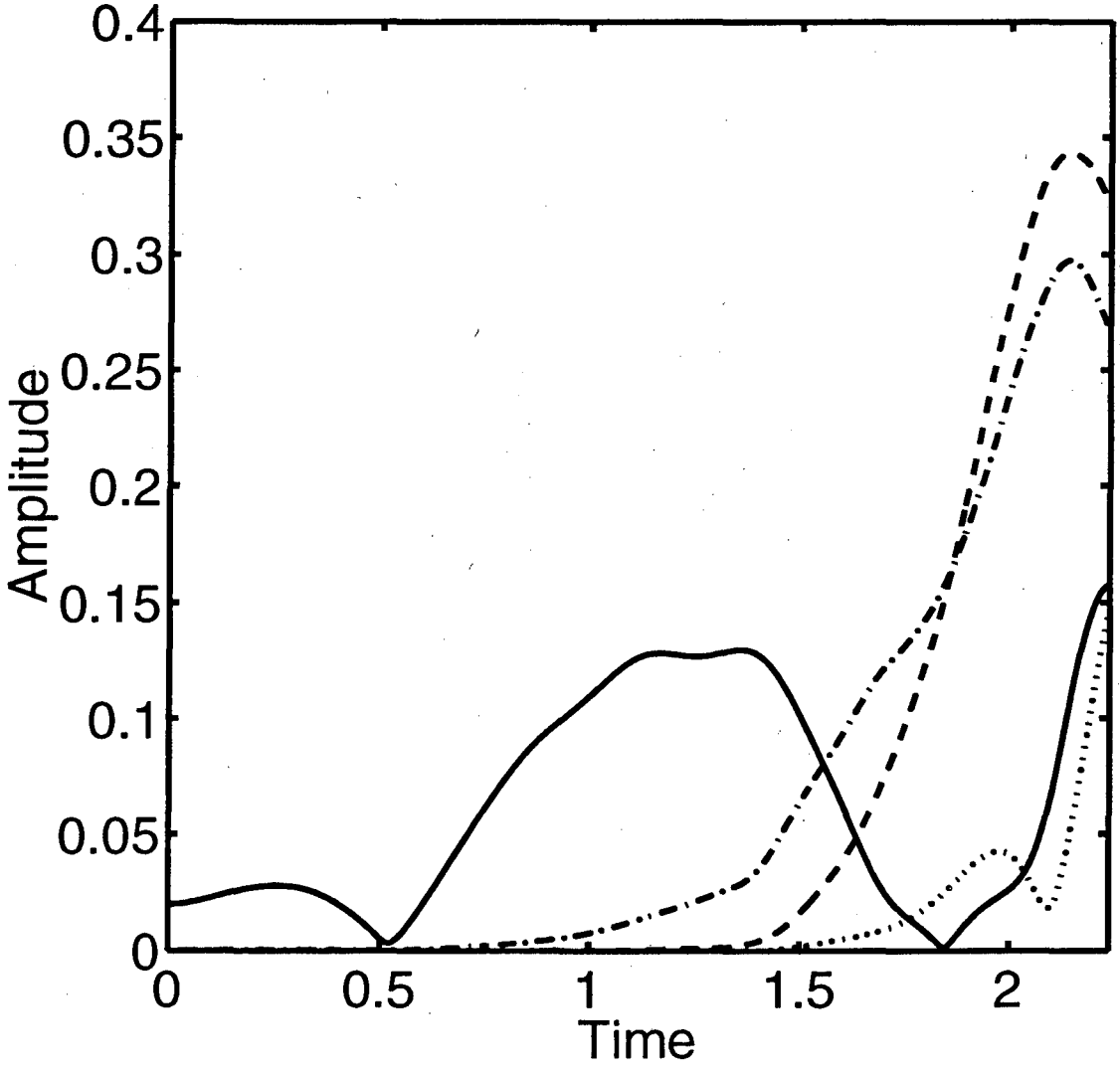

Figure 7 (a)

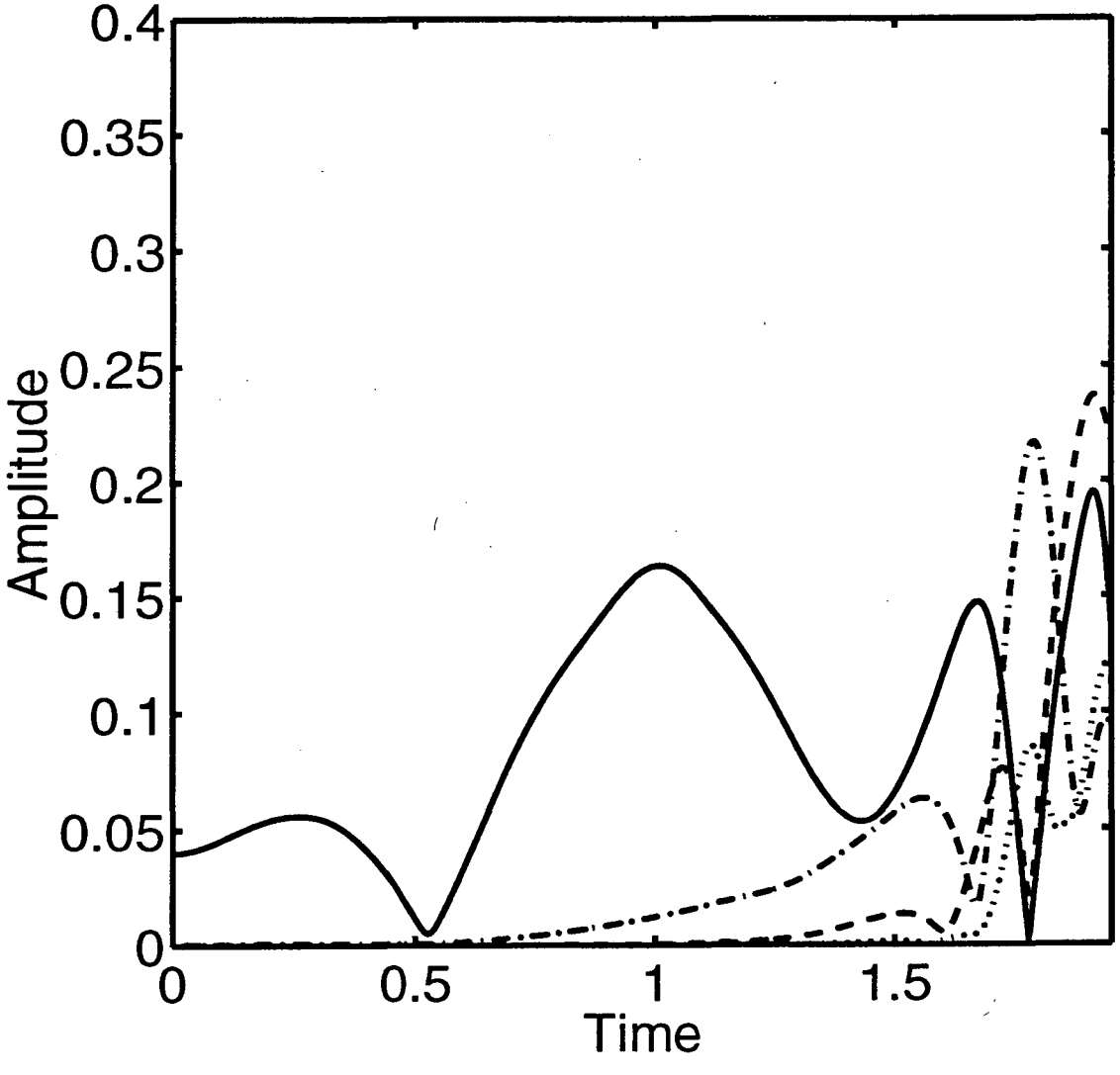

Figure 7 (b)

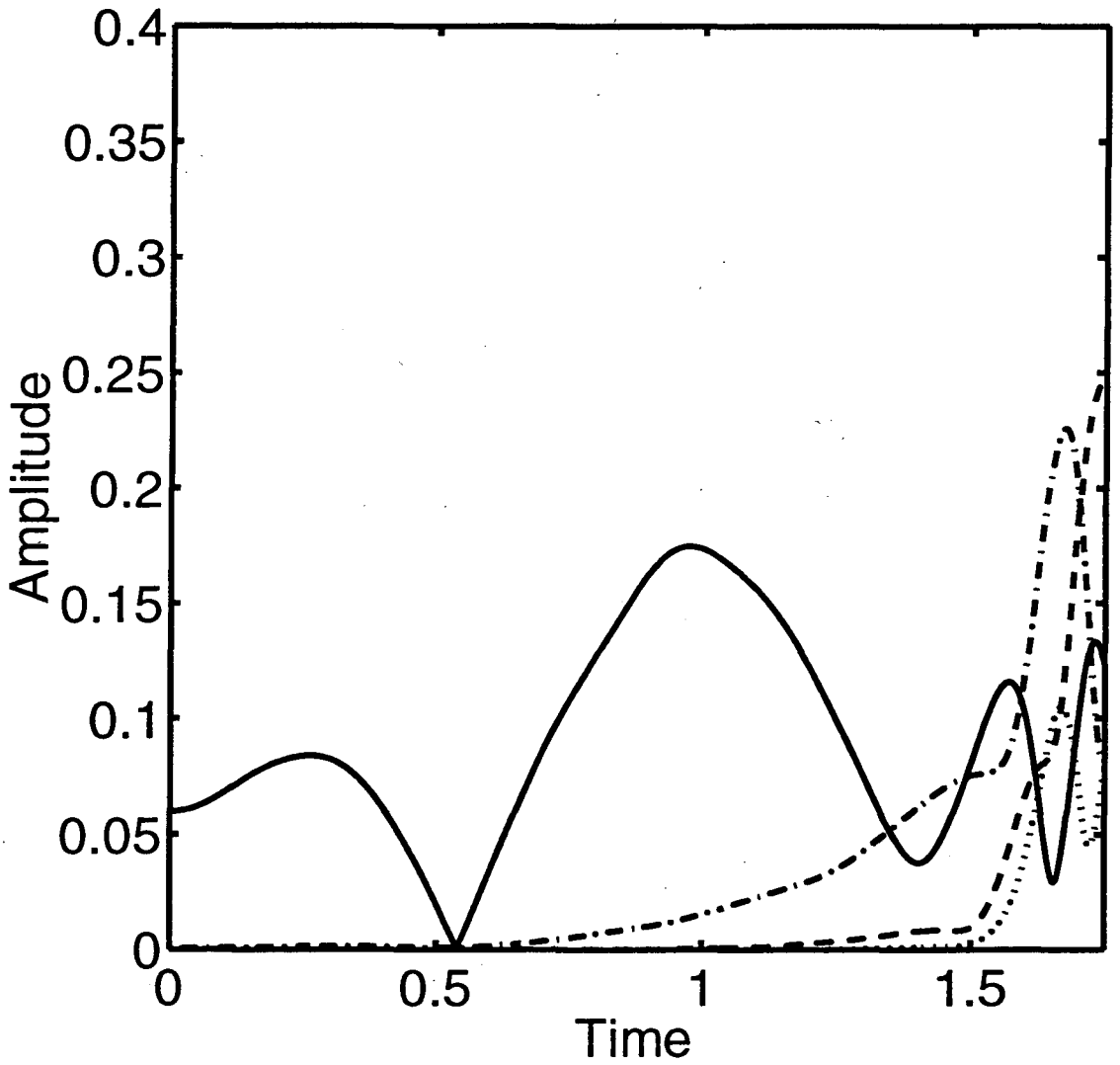

Figure 7 (c)

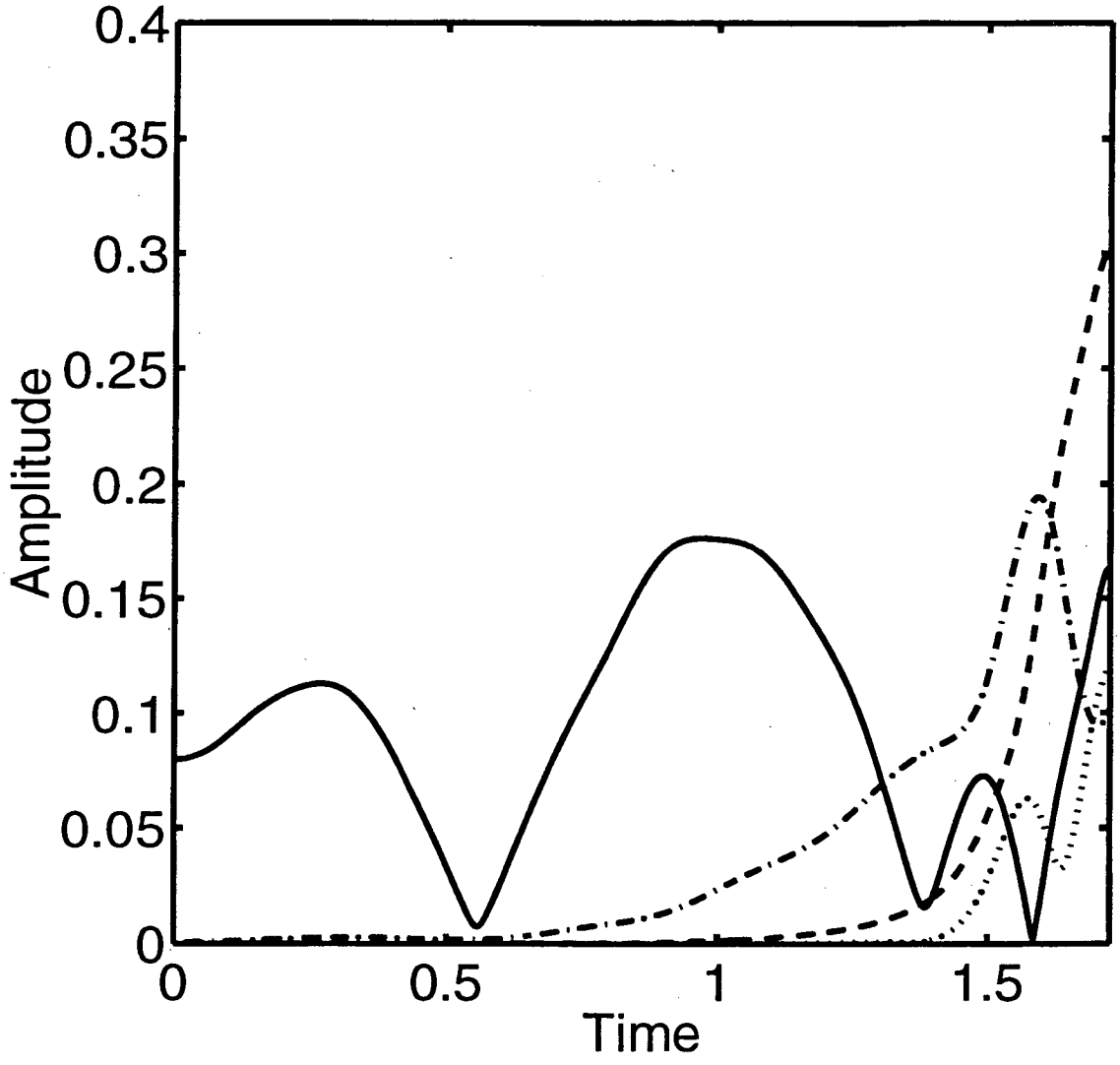

Figure 7 (d)

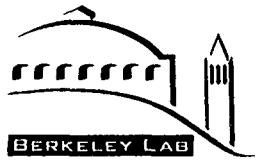

ERNEST ORLANDO LAWRENCE BERKELEY NATIONAL LABORATORY
TECHNICAL AND ELECTRONIC INFORMATION DEPARTMENT
UNIVERSITY OF CALIFORNIA | BERKELEY, CALIFORNIA 94720